

## 28. VOLCANIC ROCKS FROM THE SOUTHEAST GREENLAND MARGIN AT 63°N: COMPOSITION, PETROGENESIS, AND MANTLE SOURCES<sup>1</sup>

J.G. Fitton,<sup>2</sup> A.D. Saunders,<sup>3</sup> L.M. Larsen,<sup>4</sup> B.S. Hardarson,<sup>2</sup> and M.J. Norry<sup>3</sup>

### ABSTRACT

Early Tertiary volcanic rocks recovered from the southeast Greenland margin represent the transition from continental tholeiitic flood basalt to voluminous oceanic magmatism. This magmatism accompanied continental breakup and resulted in the formation of seaward-dipping reflector sequences (SDRS) characteristic of volcanic rifted margins. The earliest, and most landward, lava flows (Hole 917A, Lower and Middle Series) comprise a pre-breakup continental sequence ranging in composition from olivine basalt to dacite. Evolution in crustal magma reservoirs, with a dwindling supply of primitive magma and an increasing role of crustal contamination, can account for the variations in magma composition. Changes in the inferred nature of the contaminant suggest that the site of magma storage may have moved to shallower levels in the crust during the pre-breakup period. The subsequent eruption of picrite and olivine basalt magmas (Hole 917A, Upper Series) marked a dramatic change in the style of magmatism to one of unrestrained passage of primitive magma from the mantle to the surface during the final stages of breakup. The younger parts of the SDRS (Sites 915 and 918) are composed of compositionally uniform basalt ( $7.6 \pm 0.8\%$  MgO), suggesting that an effective magmatic filtering system was established, soon after breakup, in magma chambers associated with a spreading axis. An increase in degree of mantle melting (<5% to 10%–20%), accompanied by a decrease in depth of melt segregation, marked the transition from continental to oceanic volcanism. The continental volcanic rocks had a garnet lherzolite source, whereas the post-breakup magmas had a shallower, spinel lherzolite source. Most of the older basalts (Site 917, Lower to Upper Series) had a mantle source similar to that of normal mid-ocean-ridge basalt (N-MORB), although a group of flows with compositions similar to typical Icelandic basalt occurs high in the Lower Series. All the post-breakup basalt lava flows (Sites 915 and 918) had a depleted Icelandic mantle source. The head of the Iceland plume may have been zoned at the time of continental breakup with a core of Icelandic mantle surrounded by a carapace of anomalously hot N-MORB-source mantle.

### INTRODUCTION

Rifting along the North Atlantic margin was accompanied by an intense phase of basaltic magmatism, now represented by onshore flood basalt outcrops and offshore seaward-dipping reflector sequences (SDRS). The eruption of the SDRS coincided approximately with seafloor magnetic Anomaly 24R (53–56 Ma; Cande and Kent, 1992) and marked the transition from continental to oceanic volcanism. The southeast Greenland SDRS are more than 6 km thick (Larsen and Jakobsdóttir, 1988). Wide-angle seismic experiments on the conjugate margin off Rockall Plateau (Fig. 1) show that the SDRS were erupted on attenuated continental crust underlain by a prism of underplated igneous material as much as 15 km thick (White et al., 1987). These enormous volumes of magma require the presence of anomalously hot mantle at the time of rifting and continental breakup (White and McKenzie, 1989). In the case of the North Atlantic, there is a clear genetic link between the excess magmatism represented by the SDRS and the presence of a mantle plume now situated beneath Iceland.

The southeast Greenland margin provides an excellent and arguably unique area in which to investigate the link between continental rifting, large igneous provinces, and mantle plumes. The Greenland continental margin is tectonically uncomplicated and is linked across the North Atlantic to its conjugate margin by the aseismic Greenland-Iceland-Faeroes Ridge. Thus, all components of the province, from

the earliest manifestations of volcanism on the Greenland margin to present-day magmatism in Iceland, are available for study. One of the objectives of Ocean Drilling Program (ODP) Leg 152 was to sample a transect across the southeast Greenland SDRS at 63°N and to investigate the timing and character of the transition from continental to oceanic magmatism. Leg 163 extended this transect and also drilled the SDRS at 66°N (Site 988). Two previous Deep Sea Drilling Project (DSDP) and ODP legs have sampled portions of the North Atlantic SDRS. Leg 81 sampled the southern tip of the SDRS on Hatton Bank (Roberts, Schnitker, et al., 1984), and Leg 104 sampled the Vøring Plateau on the Norwegian continental margin (Eldholm, Theide, Taylor, et al., 1987; Viereck et al., 1988, 1989). The location of these drill sites is shown in Figure 1.

Holes drilled at three of the six Leg 152 sites (Holes 915A, 917A and 918D; Fig. 2) penetrated volcanic basement. A section across the SDRS, showing the location of the drill sites, is given in Figure 3. This section is based on seismic profiles and summarizes the stratigraphy of the shelf and adjacent Irminger Basin. The most landward site (Hole 917A), 50 km from the Greenland coast, was the most successful and penetrated the feather-edge of the SDRS all the way to a metasedimentary basement. A 779-m volcanic sequence comprising at least 91 flow units was recovered, although about 300 m of the lowest part of the succession was missing due to faulting. Hole 915A, 8 km farther offshore, sampled a single basalt flow at a stratigraphic level between 100 and 200 m above the top of the volcanic succession in Hole 917A. Both of these sites were on the continental shelf where the SDRS laps onto thinned continental crust. The third site from which volcanic rocks were recovered (Hole 918D) was on oceanic crust in the Irminger Basin, 130 km offshore and close to the center of the SDRS. A 121.6-m section comprising at least 18 lava flow units was recovered, the top three of which are completely altered and oxidized, implying a long period of subaerial weathering after emplacement (Holmes, this volume). The volcanic sequence is overlain by lower Eocene marine greensands intruded by a thin sill of very

<sup>1</sup>Saunders, A.D., Larsen, H.C., and Wise, S.W., Jr. (Eds.), 1998. *Proc. ODP, Sci. Results, 152*: College Station, TX (Ocean Drilling Program).

<sup>2</sup>Department of Geology and Geophysics, University of Edinburgh, West Mains Road, Edinburgh EH9 3JW, United Kingdom. godfrey.fitton@glg.ed.ac.uk

<sup>3</sup>Department of Geology, University of Leicester, University Road, Leicester LE1 7RH, United Kingdom.

<sup>4</sup>Geological Survey of Denmark and Greenland, Thoravej 8, DK-2400 Copenhagen NV, Denmark.

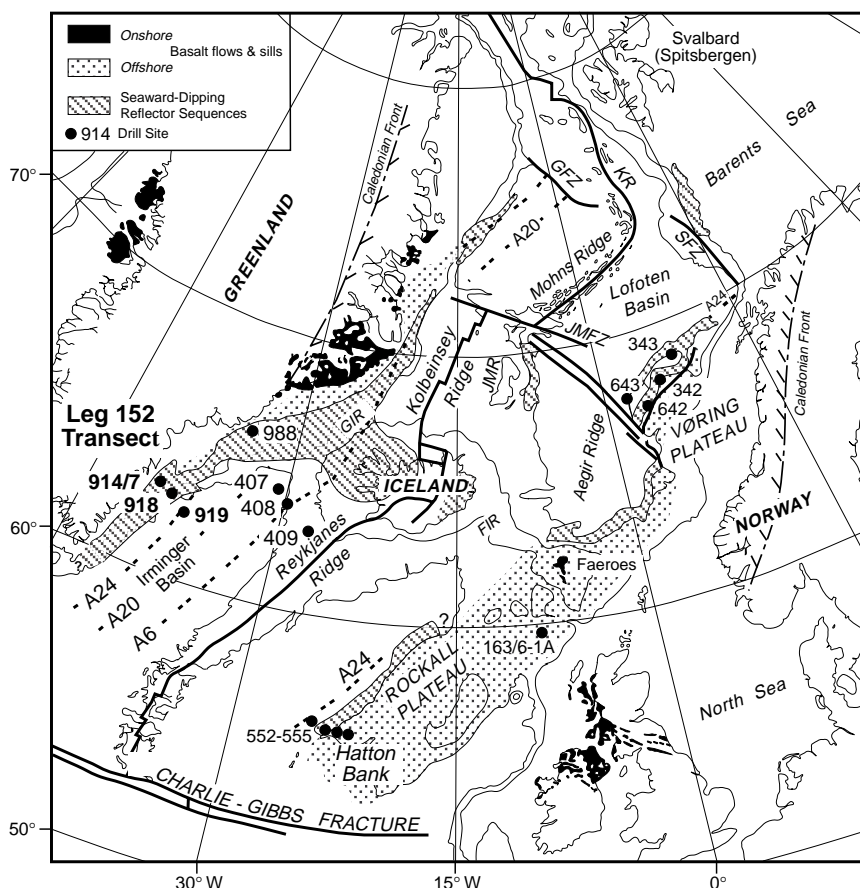


Figure 1. Map of the North Atlantic Ocean showing the main tectonic features of the region, selected seafloor magnetic anomalies, the distribution of Tertiary igneous rocks, and the location of DSDP and ODP drill sites. KR = Knipovich Ridge; GFZ = Greenland Fracture Zone; SFZ = Senja Fracture Zone; JMFZ = Jan Mayen Fracture Zone; JMR = Jan Mayen Ridge; GIR = Greenland-Iceland Ridge; and FIR = Faeroes-Iceland Ridge (after Larsen, Saunders, Clift, et al., 1994).

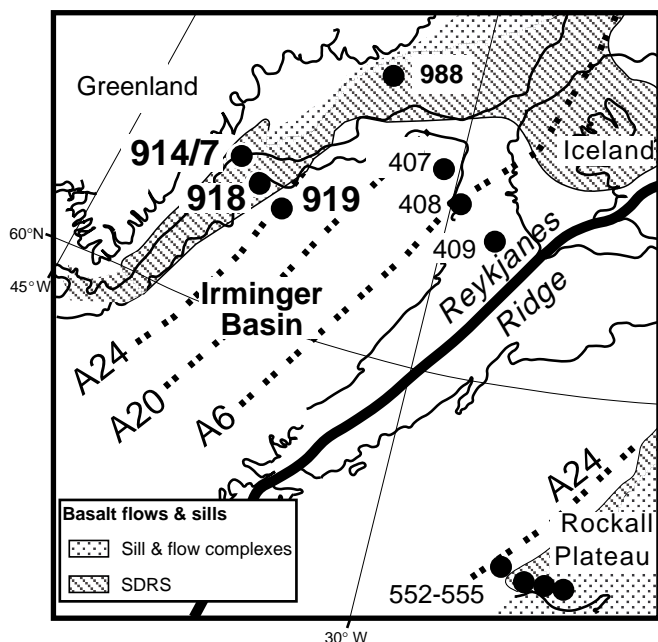


Figure 2. Map of the southeast Greenland margin and the Irminger Basin showing the location of sites drilled during ODP Legs 152 (914–919) and 163 (988), and DSDP Legs 49 (407–409) and 81 (552–555). Magnetic Anomalies 6, 20, and 24 are shown for reference.

fresh, homogeneous basalt. The lava flows sampled at the three sites show both pahoehoe and aa morphology. The flows are frequently reddened and, at Site 917, are interbedded with occasional soil horizons. Unequivocal pillow lavas and hyaloclastite breccias are rare, and it is clear that the sampled portions of the SDRS were erupted above or very close to sea level. A full description of the cores recovered during Leg 152 is given in Larsen, Saunders, Clift, et al. (1994).

This paper reports results of studies on a suite of 80 volcanic rock samples collected for analysis during Leg 152. Samples are identified by site and unit (defined in Larsen, Saunders, Clift, et al., 1994), and these informal sample numbers are keyed to full ODP designations in Table 1. A sample of Archaean gneiss, collected from an onshore outcrop close to the Leg 152 transect (GGU 324721, Blichert-Toft et al., 1995), was provided by Minik Rosing and analyzed with the Leg 152 samples. We shall document the chemical composition of the SDRS, discuss their magmatic evolution, and attempt to deduce the relative contribution of plume and nonplume mantle sources.

### ANALYTICAL TECHNIQUES

Samples were cut into small pieces with a diamond-tipped saw, and any obvious amygdalae and veins were removed. Saw marks were ground away on a diamond wheel, and the fragments were rinsed in clean water and dried before being ground to a fine powder in an agate Tema barrel. Agate was used in preference to tungsten carbide to avoid contamination with Ta and Co. The powders were analyzed in Edinburgh by X-ray fluorescence (XRF) spectrometry, and in Leicester by neutron activation analysis (NAA). A separate suite of volcanic rock samples was prepared and analyzed by XRF at the Geological Survey of Greenland for major elements, and at the University of Copenhagen for trace elements. Agreement between the Edinburgh and Copenhagen XRF data is generally very good

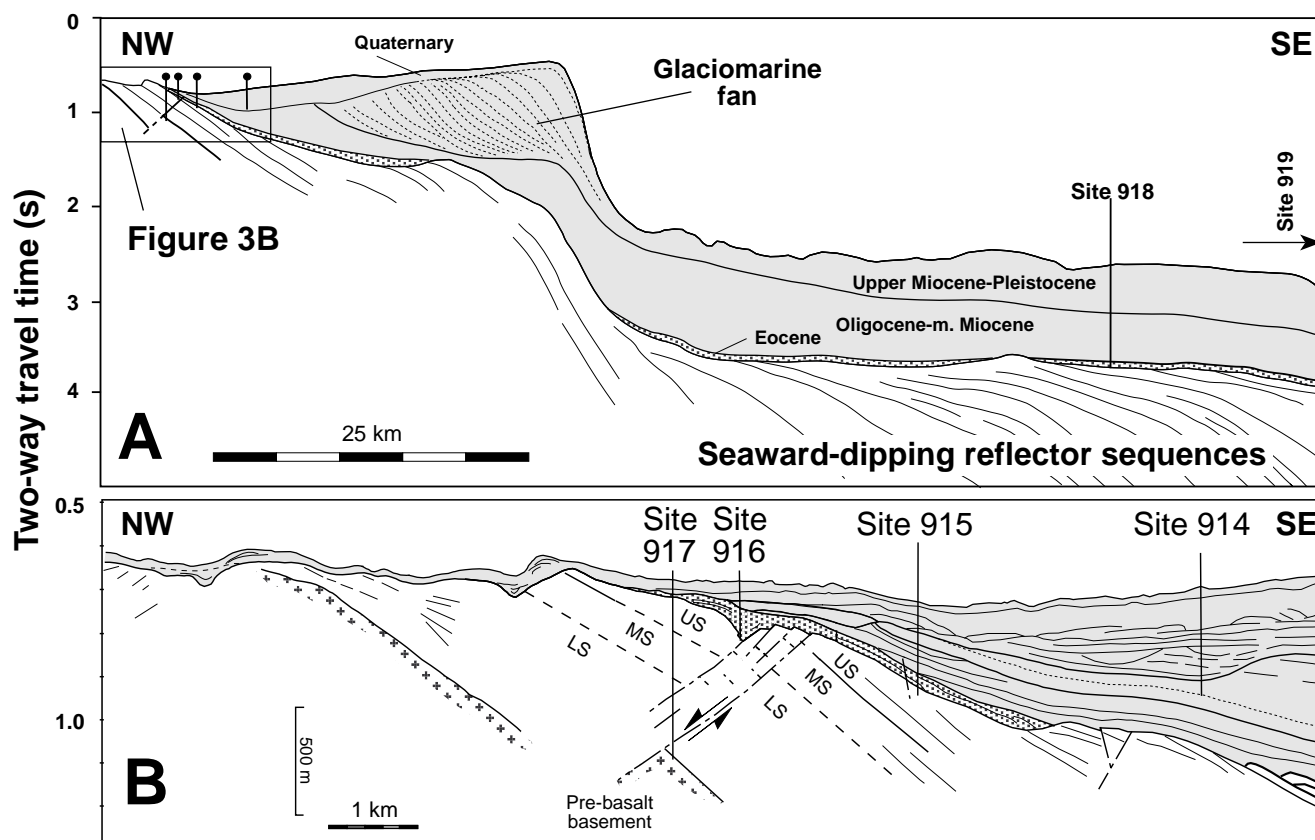


Figure 3. Interpreted seismic section across the southeast Greenland margin at 63°N, showing the location of the Leg 152 drill sites (after Leg 152 Shipboard Scientific Party, 1994).

(Larsen, Fitton, Bailey, and Kystol, this volume). The present paper is based on the Edinburgh and Leicester data.

### X-ray Fluorescence (XRF) Analysis

Major-element concentrations were determined after fusion with a lithium borate flux containing  $\text{La}_2\text{O}_3$  as a heavy absorber, by a method similar to that developed by Norrish and Hutton (1969). Rock powder was dried at 110°C for at least 1 hr, and a nominal but precisely weighed 1-g aliquot ignited at 1100°C to determine loss on ignition (LOI). The residue was then mixed with Johnson Matthey Spectroflux 105 in a sample:flux ratio of 1:5, based on the *unignited* sample mass, and fused at 1100°C in a muffle furnace in a Pt5% Au crucible. After the initial fusion, the crucible was reweighed and any flux weight loss was made up with extra flux. After a second fusion over a Meker burner, the molten mixture was swirled several times to ensure homogeneity, cast onto a graphite mold, and flattened with an aluminum plunger into a thin disk. The mold and plunger were maintained at a temperature of 220°C on a hotplate.

Trace-element concentrations were determined on pressed-powder samples. Six grams of rock powder were mixed thoroughly with four drops of a 2% aqueous solution of polyvinyl alcohol. The mixture was formed into a 38-mm disc on a 40-mm diameter polished tungsten carbide disc, backed and surrounded by boric acid, and compressed in a hydraulic press at 0.6 tons/cm<sup>2</sup>.

The fused and pressed samples were analyzed using a Philips PW 1480 automatic X-ray fluorescence spectrometer with a Rh-anode X-ray tube. Because shipboard XRF analyses showed that many of the volcanic rocks had extremely low concentrations of incompatible trace elements, the analytical conditions and calibrations for these elements were optimized for low concentrations where appropriate.

Background positions were placed as close as possible to peaks, and long count times were used at both peak and background positions. Where background count rates were measured on either side of the peak, as in most trace-element determinations, the count time was divided equally between the two positions. Analytical conditions are summarized in Table 2.

Corrections for matrix effects on the intensities of major-element lines were made using theoretical alpha coefficients calculated on-line using the Philips software. The coefficients were calculated to allow for the amount of extra flux replacing volatile components in the sample so that analytical totals should be 100% less the measured LOI. Intensities of the longer-wavelength trace-element lines (La, Ce, Nd, Cu, Ni, Co, Cr, V, Ba, and Sc) were corrected for matrix effects using alpha coefficients based on major-element concentrations measured at the same time on the powder samples. Matrix corrections were applied to the intensities of the other trace-element lines by using the count rate from the  $\text{RhK}\alpha$  Compton scatter line as an internal standard (Reynolds, 1963). Line-overlap corrections were applied using synthetic standards.

The spectrometer was calibrated with USGS and CRPG standards, using the values given by Jochum et al. (1990) for Nb and Zr, and Govindaraju (1994) for the other elements. Trace-element analytical precision was estimated by analyzing several standards repeatedly during the analysis of the Leg 152 samples. The results are shown in Table 3. Some elements (Nb at <1 ppm, Pb and Th) were determined at least three times on the Leg 152 samples, and the results averaged. The averages are thought to be precise ( $2\text{ se}$ ) to  $\pm 0.1$  ppm for Nb and  $\pm 0.5$  ppm for Pb and Th. Accuracy is more difficult to quantify but may be assessed by comparing average standard concentrations reported in Table 3 with those given by Govindaraju (1994). Major-element precision is governed more by reproducibility

**Table 1. Location of samples used in this study.**

Sample	Core, section, interval (cm)	Piece	Depth (mbsf)	Series	Unit
915-3	915A-24R-2, 60–64	2B	198.68	Lava	3
917-1	917A-6R-1, 104–108	9	42.74	Upper	1
917-2	917A-7R-2, 0–4	1	48.17	Upper	2
917-6	917A-8R-4, 5–8	1	60.10	Upper	6
917-9	917A-10R-1, 76–80	1G	74.66	Upper	9
917-10	917A-10R-4, 48–51	2A	78.53	Upper	10
917-12	917A-11R-1, 139–143	5C	84.29	Upper	12
917-13	917A-11R-4, 18–22	1B	86.94	Upper	13
917-14	917A-12R-1, 31–36	4A	92.31	Upper	14
917-16	917A-13R-2, 42–46	1B	102.97	Upper	16
917-17	917A-13R-5, 120–124	11	108.19	Upper	17
917-18	917A-14R-3, 72–77	6B	113.37	Upper	18
917-19	917A-15R-2, 28–33	1B	120.93	Upper	19
917-21	917A-16R-5, 21–25	2A	134.22	Upper	21
917-24	917A-17R-4, 141–145	8A	142.10	Upper	24
917-25	917A-18R-3, 86–89	2	149.44	Upper	25
917-26	917A-18R-4, 105–109	7B	151.04	Upper	26
917-27	917A-18R-6, 87–91	5A	153.81	Upper	27
917-31A	917A-19R-4, 59–63	3	160.18	Upper	31A
917-31B	917A-20R-1, 38–42	4	164.88	Upper	31B
917-32B	917A-20R-4, 131–134	11	170.06	Upper	32B
917-33	917A-21R-3, 126–130	5	177.75	Upper	33
917-34B	917A-23R-2, 64–68	15	194.01	Middle	34B
917-38	917A-26R-1, 135–140	17	212.15	Middle	38
917-41	917A-27R-2, 74–79	8	217.51	Middle	41
917-43	917A-30R-1, 68–71	10A	230.58	Middle	43
917-44	917A-30R-3, 44–48	7	233.09	Middle	44
917-45	917A-31R-1, 77–81	10	235.37	Middle	45
917-47	917A-32R-4, 76–80	10	244.82	Middle	47
917-49	917A-34R-1, 132–136	21	260.22	Middle	49
917-50	917A-35R-2, 8–13	1B	264.88	Middle	50
917-52	917A-42R-2, 126–130	2D	314.33	Middle	52
917-54	917A-47R-2, 80–84	8	347.96	Middle	54
917-55	917A-51R-1, 42–45	10	365.42	Middle	55
917-56	917A-53R-1, 90–98	2	375.50	Middle	56
917-57	917A-53R-2, 20–28	5	376.30	Middle	57
917-58	917A-54R-4, 70–73	1C	388.95	Lower	58
917-60	917A-55R-5, 66–70	9A	399.98	Lower	60
917-61B	917A-57R-3, 67–71	1A	416.36	Lower	61B
917-62	917A-57R-7, 29–32	1B	421.58	Lower	62
917-63	917A-58R-3, 0–5	1A	424.69	Lower	63
917-66	917A-62R-1, 46–50	5A	451.76	Lower	66
917-68	917A-64R-2, 43–47	1B	472.63	Lower	68
917-70	917A-67R-3, 126–130	6B	503.69	Lower	70
917-71	917A-69R-2, 123–127	4	521.53	Lower	71
917-72	917A-71R-4, 27–31	1C	542.07	Lower	72
917-73A	917A-72R-1, 53–57	3D	547.83	Lower	73A
917-74A	917A-74R-1, 41–48	8A	567.11	Lower	74A
917-75A	917A-76R-1, 72–78	5	582.02	Lower	75A
917-76	917A-78R-2, 135–140	4B	597.98	Lower	76
917-78	917A-79R-2, 75–79	1D	607.19	Lower	78
917-79	917A-80R-3, 102–107	1D	618.62	Lower	79
917-81B	917A-81R-4, 54–58	6	629.32	Lower	81B
917-82	917A-83R-2, 54–59	1B	645.84	Lower	82
917-83	917A-83R-7, 95–99	3	652.97	Lower	83
917-84	917A-87R-5, 38–42	1A	687.11	Lower	84
917-85	917A-90R-1, 67–70	2B	710.77	Lower	85
917-86	917A-90R-5, 63–65	1C	715.71	Lower	86
917-87	917A-92R-4, 31–35	2	727.70	Lower	87
917-88	917A-96R-1, 110–114	10A	760.50	Lower	88
917-89	917A-97R-2, 11–15	1A	770.36	Lower	89
917-90	917A-99R-2, 60–64	1D	790.37	Lower	90
917-91	917A-100R-3, 71–75	1C	801.28	Lower	91
917-92	917A-101R-4, 90–94	6A	812.33	Lower	92
918-1	918D-94R-1, 80–84	4D	1176.20	Sill	1
918-5B	918D-99R-4, 8–12	1	1209.68	Lava	5B
918-6B	918D-100R-3, 17–22	1B	1215.61	Lava	6B
918-7B	918D-101R-1, 9–12	3	1223.79	Lava	7B
918-8B	918D-101R-4, 96–100	12	1226.65	Lava	8B
918-9B	918D-103R-1, 89–93	4C	1241.39	Lava	9B
918-10B	918D-104R-2, 32–37	6A	1244.79	Lava	10B
918-11Bi	918D-105R-2, 20–24	4A	1249.25	Lava	11B
918-11Bii	918D-106R-2, 71–75	6B	1254.73	Lava	11B
918-12Bi	918D-107R-2, 92–96	12B	1259.58	Lava	12B
918-12Bii	918D-108R-1, 42–46	2B	1262.62	Lava	12B
918-13B	918D-109R-3, 50–54	5	1270.15	Lava	13B
918-14	918D-110R-4, 89–93	7B	1277.14	Lava	14
918-15	918D-111R-3, 77–81	9B	1285.12	Lava	15
918-17	918D-112R-3, 20–24	2B	1293.97	Lava	17
918-18	918D-113R-1, 116–121	12D	1301.66	Lava	18

in making the fused beads than by counting statistics. Calibration lines are excellent for all major elements so accuracy and precision are closely similar. Typical major-element precision estimates are given in Table 2.

### Neutron Activation Analysis (NAA)

Aliquots of powder (0.2 g) were accurately weighed into plastic capsules, which were sealed prior to irradiation at Silwood Park, the Imperial College Reactor Centre at Ascot. Samples and iron-foil flux monitors were given a total neutron flux of approximately  $6.2 \times 10^6$  n cm<sup>-2</sup>, by irradiating in core tube 4, positions 3 and 4, for 2 days (=  $2 \times 7.5$  hr). Samples were allowed to cool for 6 days before being counted.

Each sample was counted three times. Two counts, each of approximately 2000 s, were made within one week of irradiation. These counts provide peak spectra for La, Sm, Sc, and Co. The main count, carried out between one and four weeks after irradiation, was for a longer duration, between one-half and one day per sample. Two detectors were used: a high-energy GEM coaxial detector, with a resolution of 1.67 keV at 1.33 MeV (FWHM), for measuring La at 1596.2 keV, Sc at 889.3 keV, and Co at 1332.5 keV; and a LOAX detector with a resolution of 299 eV at 5.9 keV and 563 eV at 122 keV (FWHM) for Sm and Gd (103.2 keV), Nd (91.0 keV), Eu (123.1 keV), Tb (86.8 keV), Yb (63.1 keV), Lu (113.0 or 208.4 keV), Ta (67.7 or 100.1 keV), Hf (133.0 keV), and Th (98.4 keV).

The equipment used is EG&G hardware, with an MCA buffer emulator installed on an IBM 30 PC. Data from the two detectors are channeled through a multiplexer prior to storage in the MCA buffer. Spectra are transferred to a VAX computer for peak stripping peak-area computation using SAMPO software. Peak intensities are compared to those of known reference standards (Ailsa Craig microgranite AC-2 for most elements, JB-1a basalt for Sc and Co) for calculation of element abundances. Inter-element corrections are made where necessary (Potts, 1986, chapter 12). Flux corrections were made by counting iron foils, irradiated simultaneously with the samples.

Standards JB-1a and an internal standard, Whin Sill basalt, are used to check the accuracy of the data except for Sc and Co, which were measured using JB-1a as the monitor reference standard. Nb/Ta and Zr/Hf ratios are used to check for consistency between NAA and XRF data. With the exception of the more evolved samples from the Middle Series of Hole 917A, these ratios are chondritic. Agreement between data determined by XRF and NAA (La, Ce, Nd, Th, and Sc) is generally very good. Precision estimates are given in Table 3.

### COMPOSITION OF THE VOLCANIC ROCKS

Analytical results are given in Tables 4 (XRF data) and 5 (NAA data). The compositional range of the volcanic rocks is illustrated on primitive-mantle-normalized trace-element abundance diagrams (Figs. 4, 5), and on chondrite-normalized rare-earth element (REE) diagrams (Figs. 6, 7). The principal aim of this section is to describe the compositional variation of volcanic rocks along the transect sampled by Leg 152. The lavas range in composition from picrite to dacite and all are hypersthene-normative. A general description of the petrography, and petrographic descriptions of individual samples, are given in the Leg 152 *Initial Reports* (Larsen, Saunders, Clift, et al., 1994).

### Effects of Alteration

Alteration ranges from severe (no fresh olivine or plagioclase) to slight (olivine mostly fresh). Most samples are moderately altered, and fresh olivine is rare. Consequently the measured concentrations of the more mobile elements must be treated with caution. However,

**Table 2. X-ray fluorescence analytical conditions.**

Element	Line	Generator settings		Primary collimator	Analyzing crystal	Background offset ( $^{\circ}2\theta$ )	Detector	Line overlap	Peak and background count times (s)	Typical $1\sigma^*$
		kV	mA							
Fe	K $\alpha$	50	50	Fine	LiF200	-2.50	Flow		10	0.03%
Mn	K $\alpha$	50	50	Fine	LiF200	+2.50	Flow		10	0.007
Ti	K $\alpha$	50	50	Fine	LiF200	+3.50	Flow		20	0.006
Ca	K $\alpha$	50	50	Fine	LiF200	-4.00	Flow		20	0.03
K	K $\alpha$	50	50	Fine	LiF200	-5.00	Flow		20	0.005
P	K $\alpha$	40	60	Coarse	Ge111	+3.00	Flow		50	0.003
Si	K $\alpha$	40	60	Coarse	PE	+4.00	Flow		50	0.10
Al	K $\alpha$	40	60	Coarse	PE	-6.50	Flow		50	0.05
Mg	K $\alpha$	40	60	Coarse	PX1	+3.10	Flow		50	0.05
Na	K $\alpha$	40	60	Coarse	PX1	+6.20	Flow		50	0.05
Nb	K $\alpha$	80	30	Fine	LiF200	$\pm 0.36$	Scint.	YK $\beta_1$	500	0.1 ppm
Zr	K $\alpha$	80	30	Fine	LiF200	+0.66, -0.76	Fl.+scint.	SrK $\beta_1$	100	0.4
Y	K $\alpha$	80	30	Fine	LiF200	$\pm 0.60$	Fl.+scint.	RbK $\beta_1$	100	0.4
Sr	K $\alpha$	80	30	Fine	LiF200	$\pm 0.76$	Fl.+scint.		40	0.5
Rb	K $\alpha$	80	30	Fine	LiF200	+0.50, -0.34	Fl.+scint.		100	0.3
Th	L $\alpha_1$	80	30	Fine	LiF200	+0.22, -0.36	Scint.		500	0.4
Pb	L $\beta_1$	80	30	Fine	LiF200	$\pm 0.26$	Scint.		500	0.4
La	L $\alpha_1$	50	50	Fine	LiF200	$\pm 0.66$	Flow		500	1.0
Ce	L $\beta_1$	50	50	Fine	LiF200	+1.15, -0.64	Flow	CrK $\alpha^{\dagger}$	500	1.5
Nd	L $\alpha_1$	50	50	Fine	LiF200	+0.64, -1.15	Flow	CeL $\beta_1$ , CrK $\alpha^{\dagger}$	500	1.0
Zn	K $\alpha$	50	50	Fine	LiF200	$\pm 0.66$	Fl.+scint.		40	0.5
Cu	K $\alpha$	50	50	Fine	LiF200	+1.70, -0.70	Flow		40	0.5
Ni	K $\alpha$	50	50	Fine	LiF200	+1.30, -1.95	Flow		40	1.0
Co	K $\alpha$	50	50	Fine	LiF200	+1.20	Flow	FeK $\beta$	100	1.0
Cr	K $\alpha$	50	50	Fine	LiF200	+1.62, -0.88	Flow	VK $\beta$	40	1.0
V	K $\alpha$	50	50	Fine	LiF220	+3.54, -1.30	Flow	TiK $\beta$	40	2.0
Ba	L $\alpha_1$	50	50	Fine	Ge220	+1.60, -2.70	Flow	TiK $\alpha$ , ScK $\beta$	200	5.0
Sc	K $\alpha$	50	50	Fine	LiF200	-2.00	Flow	CaK $\beta$	100	0.5
Ga	K $\alpha$	50	50	Fine	LiF200	$\pm 0.60$	Fl.+scint.		100	0.4

Notes: \* = standard deviation: in wt% for Fe to Na, in ppm for Nb to Ga.  $\dagger$  = overlap on background position.

**Table 3. XRF and NAA trace-element data (in ppm) for international standards analyzed with the Leg 152 samples.**

XRF:	BCR-1			BIR-1			BHVO-1			W-2			DNC-1		
	Mean	$1\sigma$	n	Mean	$1\sigma$	n	Mean	$1\sigma$	n	Mean	$1\sigma$	n	Mean	$1\sigma$	n
Nb	13.3	0.1	3	0.6	0.2	3	20.1	0.1	3						
Zr	190.8	0.4	3	13.4	0.3	3	177.7	0.4	3						
Y	37.2	0.2	3	16.4	0.6	3	28.1	0.4	3						
Sr	333.7	0.4	3	110.6	0.4	3	403.0	0.9	3						
Rb	48.1	0.6	3	0.2	0.3	3	9.6	0.3	3						
Th	6.1	0.4	15				1.4	0.5	15	2.5	0.5	10	0.4	0.3	10
Pb	14.0	0.4	15				2.5	0.5	15	8.0	0.4	10	6.2	0.4	10
La	24.9	0.7	15	0.9	1.1	15	14.7	2.1	3						
Ce	53.7	1.3	15	1.0	1.8	15	39.2	0.6	3						
Nd	28.6	1.0	15	2.0	1.0	15	26.4	0.8	3						
Zn	126.3	0.5	3	69.6	0.2	3	105.1	0.6	3						
Cu	26.6	0.5	3	118.0	0.5	3	132.2	3.0	3						
Ni	14.2	0.2	3	152.8	1.0	3	114.3	1.2	3						
Co	37.7		1	52.9		1	43.3		1	48.9	1.1	6	57.0	0.8	6
Cr	28.0	1.0	3	375.0	2.0	3	287.7	0.5	3						
V	390.2	1.4	3	313.7	2.8	3	308.1	1.5	3						
Ba	682.3	6.1	3	17.3	2.0	3	133.6	3.1	3						
Sc	31.7	0.9	3	39.5	0.3	3	29.8	0.4	3						
Ga	21.9		1	16.0		1	21.3		1	18.5	0.4	6	14.7	0.4	6

**Table 3 (continued).**

NAA:	JB-1a	JB-1a	JB-1a	JB-1a	Average	$1\sigma$	JB-1a*
Run no.:	33.1.13	34.1.13	35.1.13	36.1.13			
La	37.4	37.2	37.1	36.3	36.98	0.47	38.1
Ce	66.3	61.2	63.5	62.3	63.34	2.18	66.1
Nd	25.3	23.1	25.5	25.4	24.81	1.18	25.5
Sm	5.11	5.11	5.10	4.95	5.07	0.08	5.07
Eu	1.55	1.51	1.48	1.49	1.51	0.03	1.47
Gd				5.80	5.80		4.54
Tb	0.66	0.59	0.79	0.77	0.70	0.09	0.69
Yb	2.14	2.04	2.08	2.17	2.11	0.06	2.10
Lu	0.27	0.22	0.27	0.35	0.28	0.05	0.32
Ta	1.62	1.56	1.65	1.63	1.62	0.04	2.00
Th	9.69	8.94	9.45	9.40	9.37	0.31	8.80
Hf	3.65	3.50	3.62	3.61	3.60	0.07	3.48
U	1.98	1.98	1.82	1.76	1.89	0.11	1.60

Notes: Sc and Co INAA data are not included because JB 1a was used as the reference monitor for these two elements. \* = values from Govindaraju (1994).

**Table 4. XRF data for volcanic rocks from Leg 152, and a sample of Precambrian basement gneiss (major elements in wt%; trace elements in ppm).**

Sample: Series:	915-3 Lava	917-1 Upper	917-2 Upper	917-6 Upper	917-9 Upper	917-10 Upper	917-12 Upper	917-13 Upper	917-14 Upper	917-16 Upper	917-17 Upper	917-18 Upper	917-19 Upper	917-21 Upper
SiO <sub>2</sub>	49.76	44.80	43.85	44.77	44.76	45.69	44.91	47.19	45.28	43.38	47.90	47.64	45.71	40.13
Al <sub>2</sub> O <sub>3</sub>	14.10	15.94	10.10	14.77	14.64	14.39	14.69	14.75	12.54	11.97	15.20	15.03	14.40	9.25
Fe <sub>2</sub> O <sub>3</sub> *	13.15	12.26	12.89	12.42	11.82	11.95	12.15	11.66	10.98	11.32	11.77	11.33	12.32	10.26
MgO	7.43	9.07	18.26	9.75	11.13	10.56	11.26	9.39	14.72	16.58	8.37	8.54	9.68	23.29
CaO	11.17	9.68	5.54	9.79	8.87	9.77	9.30	10.89	8.36	6.82	10.72	10.80	10.26	2.10
Na <sub>2</sub> O	2.08	2.42	1.40	2.03	2.31	2.26	1.99	2.02	1.53	1.47	2.46	2.40	2.23	1.31
K <sub>2</sub> O	0.214	0.302	0.142	0.226	0.210	0.174	0.366	0.068	0.062	0.212	0.148	0.177	0.187	0.034
TiO <sub>2</sub>	0.914	1.080	0.690	1.309	1.097	1.153	1.087	1.161	0.753	0.841	1.403	1.241	1.416	0.828
MnO	0.198	0.158	0.175	0.199	0.183	0.207	0.194	0.185	0.182	0.219	0.172	0.170	0.198	0.149
P <sub>2</sub> O <sub>5</sub>	0.068	0.080	0.044	0.088	0.073	0.079	0.062	0.076	0.039	0.057	0.107	0.096	0.088	0.057
LOI	1.29	4.17	6.79	5.00	4.88	3.93	4.12	2.13	5.40	6.94	1.66	2.71	3.52	12.63
Total	100.37	99.96	99.88	100.35	99.97	100.16	100.13	99.52	99.85	99.81	99.91	100.13	100.01	100.04
Nb	1.8	1.4	0.7	1.2	1.0	0.9	1.1	0.8	0.3	1.0	2.2	2.1	1.9	1.3
Zr	47.6	57.8	35.7	63.1	51.7	55.7	48.9	54.8	34.9	44.5	83.8	75.4	69.8	50.6
Y	26.2	23.0	13.2	25.6	23.1	22.9	22.2	22.9	20.4	18.4	28.6	25.9	24.9	14.5
Sr	76.1	185.4	63.6	144.1	151.0	124.0	119.1	132.3	56.2	167.2	148.6	142.6	143.6	23.8
Rb	3.4	1.6	2.3	1.4	1.6	0.8	1.9	0.5	0.8	1.9	0.5	1.2	1.1	0.3
Th	0.7	0.5	0.3	0.6	0.4	0.5	0.4	0.3	0.4	0.8	0.9	0.4	0.5	0.1
Pb	0.7	0.7	0.4	0.3	0.6	0.3	0.2	0.2	0.1	0.2	1.4	1.3	0.6	0.1
La	2	3	3	2	4	3	1	3	1	2	6	6	3	2
Ce	9	12	5	7	4	7	7	7	3	8	15	15	11	5
Nd	6	8	6	7	6	7	6	7	4	6	13	10	11	5
Zn	90	76	80	75	73	79	79	76	70	71	84	78	79	65
Cu	107	99	70	141	88	90	118	111	64	165	95	83	103	87
Ni	76	389	1430	159	241	231	237	217	789	815	127	171	164	1136
Co	46	65	101	54	56	54	56	55	76	75	49	48	52	82
Cr	145	921	1695	335	429	441	462	454	1135	1310	283	344	350	1156
V	319	277	160	306	270	284	276	291	228	200	327	308	348	198
Ba	28	36	21	24	43	14	21	7	13	36	60	73	16	9
Sc	48	28	21	36	30	29	33	33	26	22	39	34	39	22
Ga	16	18	12	20	18	18	17	18	13	13	19	18	20	14

Notes: \* = total Fe as Fe<sub>2</sub>O<sub>3</sub>; † = ICP-MS data from Blichert-Toft et al. (1995).**Table 4 (continued).**

Sample: Series:	917-24 Upper	917-25 Upper	917-26 Upper	917-27 Upper	917-31A Upper	917-31B Upper	917-32B Upper	917-33 Upper	917-34B Middle	917-38 Middle	917-41 Middle	917-43 Middle	917-44 Middle	917-45 Middle
SiO <sub>2</sub>	46.59	45.30	45.77	44.69	45.54	43.41	43.97	47.16	50.32	52.18	53.27	52.45	55.75	55.68
Al <sub>2</sub> O <sub>3</sub>	14.67	12.48	13.21	12.82	13.27	11.13	10.55	14.38	13.34	15.33	15.69	15.48	15.23	14.31
Fe <sub>2</sub> O <sub>3</sub> *	11.66	13.17	12.78	12.43	12.97	12.71	11.03	12.59	15.24	11.44	10.88	11.18	10.40	11.16
MgO	8.77	13.16	10.21	11.01	11.40	16.68	22.83	8.53	5.11	5.65	5.10	5.87	4.28	4.67
CaO	11.09	7.97	9.62	9.57	8.80	6.45	6.57	9.11	9.10	7.48	7.47	8.16	5.93	5.54
Na <sub>2</sub> O	2.17	1.90	2.19	1.94	2.03	1.51	1.15	2.10	3.24	3.62	3.51	3.34	3.71	3.80
K <sub>2</sub> O	0.084	0.143	0.131	0.183	0.249	0.174	0.115	1.048	0.739	0.755	0.698	0.496	0.710	0.885
TiO <sub>2</sub>	1.312	1.654	1.796	1.713	1.749	1.325	0.713	1.443	2.474	1.261	1.193	1.391	1.156	1.128
MnO	0.158	0.211	0.194	0.171	0.202	0.174	0.173	0.213	0.358	0.163	0.141	0.238	0.161	0.203
P <sub>2</sub> O <sub>5</sub>	0.089	0.138	0.159	0.143	0.156	0.107	0.048	0.097	0.218	0.186	0.171	0.165	0.286	0.264
LOI	2.93	4.03	3.93	5.02	3.64	5.98	3.10	3.49	0.00	1.47	1.55	1.25	2.35	2.06
Total	99.52	100.16	99.99	99.69	100.01	99.65	100.25	100.16	100.14	99.54	99.67	100.02	99.96	99.70
Nb	1.9	3.9	4.3	3.9	3.6	2.8	1.3	2.3	5.7	5.1	5.0	5.3	7.1	6.8
Zr	68.3	89.8	113.1	97.7	90.7	67.3	36.6	79.4	146.9	139.4	138.4	147.3	207.0	201.5
Y	23.7	27.9	32.8	30.7	30.1	22.6	12.5	23.6	38.5	21.8	21.0	24.2	22.3	20.0
Sr	147.3	124.4	149.8	139.6	136.9	93.0	95.8	136.3	326.4	441.2	505.9	392.6	530.1	536.5
Rb	0.5	3.4	1.1	5.0	7.8	5.4	3.1	8.8	9.4	9.7	9.6	6.8	14.0	15.7
Th	0.5	0.3	0.6	0.5	0.3	0.7	0.1	0.1	3.3	2.3	2.4	2.2	3.5	2.8
Pb	0.2	1.1	0.5	0.6	1.3	0.3	0.2	0.8	5.1	4.1	6.1	4.5	9.1	9.2
La	3	5	4	5	4	3	2	2	16	25	28	22	44	41
Ce	12	17	18	16	17	12	4	11	42	60	65	47	100	90
Nd	9	14	15	15	14	12	6	10	25	27	29	24	42	40
Zn	77	91	89	90	90	82	67	82	117	89	81	104	95	113
Cu	126	97	136	87	119	132	81	138	47	77	61	100	25	29
Ni	128	534	350	367	392	847	1157	139	27	40	40	47	13	11
Co	50	65	57	55	57	77	86	50	38	41	38	42	28	30
Cr	297	788	557	625	649	1058	1762	324	44	28	29	27	8	9
V	316	321	372	337	338	255	171	341	594	299	278	320	215	249
Ba	18	33	24	28	32	18	34	141	316	468	569	630	573	591
Sc	35	24	32	29	28	22	21	40	36	33	36	39	24	21
Ga	19	17	20	19	19	15	12	19	24	21	21	21	22	21

attempts to relate compositional variation to indices of alteration, such as LOI, have generally shown no correlation, and mobile elements (Ba, Sr, K, Rb) generally correlate well with more immobile element (e.g., Zr) concentrations. Some of the irregularities in the abundance patterns in Figures 4 and 5 (notably in K and Pb) may be due to the effects of alteration, but the patterns generally show good coherence between mobile and immobile elements. We believe, therefore, that the measured concentrations generally reflect those of the original magmas, but we shall base our conclusions on the more immobile elements wherever possible.

The only rocks in which unequivocal evidence of element mobility has been found are the lavas from Site 918. Four samples with more than 2% LOI (918-6B, -11Bi, -17, and -18) have apparently lost large amounts of Ca and gained a small amount of Sc. Sample 918-18 (Table 4), with 5% LOI, has only 3.3% CaO compared with about 10% in fresher samples, and it has the highest Sc content. These four samples have been omitted from most of the data plots used in this paper. No significant correlations between LOI and other elements are seen, nor is this effect seen in samples from other sites. More surprisingly, Y appears to be mobile in the lava samples from Site 918.

Table 4 (continued).

Sample: Series:	917-47 Middle	917-49 Middle	917-50 Middle	917-52 Middle	917-54 Middle	917-55 Middle	917-56 Middle	917-57 Middle	917-58 Lower	917-60 Lower	917-61B Lower	917-62 Lower	917-63 Lower	917-66 Lower
SiO <sub>2</sub>	60.50	54.02	50.76	52.57	63.01	64.89	62.04	64.24	49.17	48.26	44.34	44.48	48.39	49.52
Al <sub>2</sub> O <sub>3</sub>	14.86	15.04	15.91	14.37	15.08	13.32	13.41	13.14	15.80	14.84	13.61	15.79	15.25	15.58
Fe <sub>2</sub> O <sub>3</sub> *	7.85	11.57	10.82	12.68	5.50	5.77	9.20	7.61	10.44	11.94	10.98	10.24	10.70	10.61
MgO	2.67	4.67	6.44	5.81	3.32	3.04	1.68	1.74	7.62	8.27	14.42	12.13	8.75	7.04
CaO	4.78	6.44	9.47	8.91	4.11	4.42	4.04	3.38	11.42	11.77	9.01	9.58	10.95	11.51
Na <sub>2</sub> O	4.21	3.60	3.37	3.09	3.80	3.62	4.06	4.49	2.51	2.39	1.71	2.03	2.33	2.64
K <sub>2</sub> O	1.571	0.624	0.222	0.835	2.126	2.992	2.840	2.918	0.161	0.159	0.172	0.464	0.122	0.235
TiO <sub>2</sub>	0.988	1.250	1.440	1.390	0.757	0.737	1.283	1.160	1.061	1.566	0.961	0.896	0.943	1.165
MnO	0.139	0.194	0.318	0.208	0.105	0.137	0.094	0.134	0.156	0.173	0.162	0.166	0.167	0.164
P <sub>2</sub> O <sub>5</sub>	0.266	0.283	0.161	0.160	0.040	0.068	0.307	0.288	0.101	0.131	0.110	0.102	0.077	0.107
LOI	1.93	1.82	0.98	0.05	2.35	0.53	0.80	0.78	1.68	0.81	4.65	3.99	2.30	1.36
Total	99.76	99.51	99.89	100.07	100.20	99.52	99.75	99.88	100.12	100.31	100.13	99.87	99.98	99.93
Nb	7.5	6.5	3.7	3.7	14.5	11.6	9.7	10.1	1.9	7.3	5.2	5.2	1.6	2.0
Zr	217.5	190.6	113.6	114.1	436.2	318.6	264.5	286.8	58.9	93.6	50.3	45.5	53.8	68.0
Y	18.8	23.2	25.3	27.0	36.7	30.1	28.4	27.7	20.0	25.9	14.3	12.8	17.3	21.8
Sr	521.5	569.9	416.1	375.3	174.4	112.0	403.5	350.7	287.3	199.3	167.1	315.9	247.9	280.9
Rb	38.3	8.5	1.7	15.9	16.0	51.3	44.7	51.0	0.7	1.2	2.0	8.3	0.2	1.3
Th	3.2	2.2	1.1	0.8	4.2	3.1	2.9	2.9	0.6	1.4	0.6	0.5	0.3	0.9
Pb	9.5	8.1	2.9	2.9	14.6	11.3	10.2	10.8	1.1	1.3	0.6	0.2	1.5	1.4
La	41	39	14	14	61	45	43	43	7	6	6	6	6	5
Ce	94	85	38	31	139	99	99	105	20	18	11	7	19	19
Nd	38	38	20	19	58	44	46	47	13	13	7	6	10	12
Zn	90	105	103	100	110	85	109	126	72	77	67	64	73	80
Cu	17	26	189	70	38	52	21	16	114	129	57	93	117	114
Ni	12	14	55	43	35	44	12	10	145	182	463	339	181	158
Co	22	34	53	46	14	17	24	24	46	49	67	57	51	48
Cr	9	9	24	19	60	73	3	4	285	377	644	580	348	255
V	165	277	360	297	118	122	174	175	281	340	182	181	238	283
Ba	833	607	206	329	1207	1020	1112	1177	140	71	79	1024	111	144
Sc	18	22	38	35	21	19	20	18	31	39	21	23	29	35
Ga	20	23	23	22	19	19	22	21	19	20	14	16	17	20

Table 4 (continued).

Sample: Series:	917-68 Lower	917-70 Lower	917-71 Lower	917-72 Lower	917-73A Lower	917-74A Lower	917-75A Lower	917-76 Lower	917-78 Lower	917-79 Lower	917-81B Lower	917-82 Lower	917-83 Lower	917-84 Lower
SiO <sub>2</sub>	48.67	51.15	51.88	51.60	44.78	54.69	53.06	46.47	47.60	48.03	48.90	48.70	46.87	49.02
Al <sub>2</sub> O <sub>3</sub>	15.35	15.33	15.37	15.69	13.04	13.31	13.47	15.42	14.55	15.79	16.29	15.96	15.53	15.68
Fe <sub>2</sub> O <sub>3</sub> *	11.04	10.79	10.07	10.34	11.97	13.94	14.61	9.64	10.24	10.88	10.27	10.57	10.55	10.12
MgO	8.32	5.55	6.95	4.93	11.79	2.98	3.71	7.70	11.38	8.13	7.61	7.69	8.95	8.65
CaO	11.24	10.05	10.04	7.71	9.28	6.25	6.98	9.38	9.39	9.67	9.99	10.18	9.27	10.83
Na <sub>2</sub> O	2.17	3.10	2.86	3.83	1.70	3.87	3.71	2.55	2.06	2.61	2.71	2.59	2.59	2.58
K <sub>2</sub> O	0.350	0.741	0.565	1.959	0.242	1.354	0.649	0.458	0.098	0.340	0.291	0.314	0.198	0.297
TiO <sub>2</sub>	1.350	1.425	1.201	2.088	1.407	2.116	1.990	1.045	0.747	1.099	1.109	1.054	1.074	0.997
MnO	0.179	0.151	0.156	0.176	0.210	0.224	0.204	0.143	0.189	0.163	0.139	0.163	0.169	0.163
P <sub>2</sub> O <sub>5</sub>	0.149	0.194	0.135	0.488	0.109	0.449	0.373	0.123	0.114	0.143	0.142	0.139	0.142	0.132
LOI	1.19	1.31	0.96	1.21	5.11	0.39	0.96	6.93	3.75	3.02	2.72	2.19	4.55	1.83
Total	100.01	99.79	100.19	100.02	99.64	99.57	99.72	99.86	100.12	99.88	100.17	99.55	99.89	100.30
Nb	9.2	15.5	3.5	61.7	2.5	10.4	9.1	2.7	2.5	3.0	3.2	2.8	2.9	2.1
Zr	100.5	143.6	116.2	298.9	75.1	288.4	258.5	70.8	47.5	78.2	78.1	71.1	66.9	61.1
Y	21.9	25.8	24.7	36.9	24.3	43.5	40.1	22.0	17.4	23.0	23.8	23.1	21.7	21.1
Sr	238.3	344.3	281.5	358.4	195.9	412.0	426.1	508.1	266.2	412.8	336.6	304.3	380.6	334.9
Rb	3.7	5.2	4.1	43.2	5.0	12.1	7.7	8.3	1.0	1.9	1.2	2.0	1.2	1.7
Th	1.8	1.5	0.4	5.5	0.5	1.4	0.9	0.3	0.4	0.3	0.4	0.4	0.2	0.3
Pb	1.7	3.2	2.3	3.1	0.5	10.2	8.1	1.1	1.9	2.0	1.6	1.7	1.8	1.9
La	8	18	13	38	4	34	34	7	7	9	9	9	9	9
Ce	21	41	28	82	8	85	79	22	21	24	23	24	24	23
Nd	11	23	16	38	10	45	41	15	12	13	14	13	15	13
Zn	79	72	80	94	76	133	135	76	70	82	85	76	80	74
Cu	101	68	81	54	134	35	35	105	98	108	95	83	93	104
Ni	114	69	90	33	366	19	21	190	291	183	180	170	179	181
Co	42	41	42	30	55	36	39	45	54	49	47	46	46	44
Cr	312	84	66	25	717	13	12	301	612	171	156	137	150	346
V	269	269	259	264	302	347	347	243	203	242	249	245	256	241
Ba	154	384	297	602	677	839	684	645	128	261	234	272	191	200
Sc	34	31	35	18	30	28	29	26	27	27	27	30	33	33
Ga	17	20	20	23	18	24	24	15	18	19	19	19	18	18

Comparison of Edinburgh and Copenhagen analytical data showed a poor interlaboratory correlation for Y in these rocks, but only when different samples of the same volcanic units were compared. Analyses of Y on aliquots of the same powder gave excellent agreement, as did other elements analyzed in different samples from Site 918. The implication is that Y is mobile during alteration, although there is no correlation between LOI and Y content, or between LOI and the difference in Y content in samples from the same volcanic unit. The difference in Y between samples, however, seems to be less for samples collected close to each other. This effect is discussed in more detail by Larsen, Fitton, Bailey, and Kystøl (this volume).

### Volcanic Stratigraphy

Stratigraphic variation is summarized in a series of diagrams (Figs. 8–10) in which composition is plotted against stratigraphic position for each of the three sites at which volcanic basement was penetrated. The vertical axis on each diagram represents time, although it must be stressed that the sequence is not continuous. The single sample from Site 915 lies at a stratigraphic level between 100 and 200 m above the top of the volcanic succession at Site 917, whereas Sites 915 and 918 are separated by a horizontal distance of 70 km (Fig. 3). Individual data points for Sites 917 and 918 were plot-

Table 4 (continued).

Sample: Series:	917-85 Lower	917-86 Lower	917-87 Lower	917-88 Lower	917-89 Lower	917-90 Lower	917-91 Lower	917-92 Lower	918-1 Sill	918-5B Lava	918-6B Lava	918-7B Lava	918-8B Lava	918-9B Lava
SiO <sub>2</sub>	46.34	47.26	46.73	44.04	47.32	47.18	47.53	48.29	48.61	49.50	47.46	49.59	49.80	49.65
Al <sub>2</sub> O <sub>3</sub>	15.12	15.41	15.59	13.41	16.05	15.81	16.08	15.49	13.26	14.99	17.27	13.48	14.33	14.35
Fe <sub>2</sub> O <sub>3</sub> *	10.54	10.64	10.29	12.06	10.59	11.42	9.90	9.73	14.93	11.84	13.17	15.51	14.19	12.63
MgO	9.06	9.01	7.93	14.43	7.34	8.44	7.29	8.81	5.76	7.85	8.18	6.84	7.16	8.16
CaO	10.78	10.89	10.08	7.99	10.86	10.39	12.52	11.17	10.75	10.32	6.46	9.04	9.25	9.84
Na <sub>2</sub> O	2.17	2.22	2.57	1.52	2.46	2.25	2.43	2.28	2.71	2.44	2.80	2.40	2.64	2.33
K <sub>2</sub> O	0.185	0.211	0.236	0.106	0.219	0.233	0.098	0.129	0.601	0.079	0.144	0.284	0.115	0.073
TiO <sub>2</sub>	0.961	0.988	1.105	1.163	1.184	1.135	1.090	1.061	2.904	1.144	1.294	1.292	1.322	1.161
MnO	0.174	0.177	0.157	0.186	0.165	0.199	0.188	0.194	0.220	0.274	0.262	0.287	0.231	0.280
P <sub>2</sub> O <sub>5</sub>	0.112	0.114	0.166	0.098	0.154	0.152	0.145	0.133	0.356	0.072	0.079	0.086	0.098	0.081
LOI	4.44	3.47	5.00	5.31	3.37	2.67	2.54	2.51	-0.21	1.17	3.12	0.92	0.92	1.22
Total	99.88	100.39	99.85	100.31	99.71	99.88	99.81	99.80	99.89	99.68	100.24	99.73	100.06	99.78
Nb	1.4	1.3	3.1	2.9	1.9	1.6	1.7	3.0	30.5	2.0	1.7	2.3	2.9	2.3
Zr	45.9	46.7	66.5	65.4	64.9	63.7	67.4	54.7	206.3	52.0	56.6	62.3	65.2	55.5
Y	20.5	20.1	22.0	20.2	22.8	22.7	21.0	21.7	45.7	26.1	33.6	34.5	52.0	26.5
Sr	420.1	420.1	639.7	157.8	501.1	332.3	393.2	334.3	249.6	93.1	98.4	82.0	99.1	94.2
Rb	2.4	0.9	1.9	0.8	3.0	5.0	0.4	0.9	11.2	0.8	0.5	3.6	0.8	0.0
Th	0.2	0.6	0.4	0.2	0.6	0.2	0.5	0.5	2.2	0.6	0.5	0.7	0.1	0.6
Pb	1.0	1.6	1.6	0.5	1.7	1.6	1.5	0.8	4.3	0.1	0.1	0.1	0.4	0.5
La	5	6	8	3	8	8	9	9	20	1	1	1	2	1
Ce	17	20	29	11	22	21	24	19	55	10	6	4	11	5
Nd	12	13	17	9	14	13	17	12	32	8	7	6	8	7
Zn	74	74	76	71	78	75	77	77	124	100	103	108	118	94
Cu	76	80	35	52	64	100	103	107	246	213	237	106	220	197
Ni	205	203	264	537	132	117	154	290	63	82	116	59	69	75
Co	52	50	52	70	46	47	51	52	43	56	87	57	62	53
Cr	455	454	493	892	298	289	338	795	102	137	231	67	84	148
V	223	232	245	205	246	268	253	245	412	394	473	407	421	388
Ba	245	190	319	56	620	1091	153	147	145	9	4	8	17	14
Sc	29	27	26	25	30	33	33	31	36	61	80	58	62	62
Ga	17	17	17	18	16	18	19	18	21	18	22	19	20	17

Table 4 (continued).

Sample: Series:	918-10B Lava	918-11Bi Lava	918-11Bii Lava	918-12Bi Lava	918-12Bii Lava	918-13B Lava	918-14 Lava	918-15 Lava	918-17 Lava	918-18 Lava	324721 Gneiss
SiO <sub>2</sub>	50.29	47.41	50.60	50.33	50.23	50.16	50.25	49.82	49.44	49.93	63.64
Al <sub>2</sub> O <sub>3</sub>	13.76	15.25	13.22	13.75	13.70	14.69	13.99	13.87	14.08	14.64	16.95
Fe <sub>2</sub> O <sub>3</sub> *	14.91	16.67	15.20	13.33	13.13	12.37	13.73	14.24	12.62	14.38	4.21
MgO	6.68	7.47	7.11	7.64	7.85	6.98	6.90	6.95	9.89	8.52	1.61
CaO	9.28	5.74	9.94	11.04	11.46	10.88	10.81	10.34	7.82	3.26	3.39
Na <sub>2</sub> O	2.36	2.82	2.34	2.11	2.05	2.39	2.41	2.36	2.44	2.23	4.15
K <sub>2</sub> O	0.241	0.152	0.072	0.128	0.065	0.149	0.127	0.081	0.086	0.414	3.921
TiO <sub>2</sub>	1.243	1.407	1.164	0.956	0.945	1.211	1.228	1.350	1.015	1.103	0.777
MnO	0.273	0.093	0.235	0.195	0.258	0.231	0.169	0.292	0.237	0.225	0.056
P <sub>2</sub> O <sub>5</sub>	0.085	0.081	0.082	0.060	0.060	0.084	0.093	0.106	0.083	0.067	0.339
LOI	1.17	2.65	0.39	0.46	0.43	0.59	0.63	0.50	2.24	4.99	0.32
Total	100.29	99.74	100.35	100.00	100.18	99.74	100.34	99.91	99.95	99.76	99.36
Nb	2.5	2.6	2.5	1.6	1.7	3.4	3.1	3.1	1.7	1.8	11.4
Zr	59.7	65.6	56.6	42.2	40.9	61.0	61.0	67.6	44.3	47.1	333.1
Y	33.0	56.4	30.1	24.5	23.9	25.3	37.2	39.2	36.7	23.3	16.0
Sr	86.9	97.7	87.0	77.9	80.2	95.2	94.9	92.2	87.2	74.7	946.7
Rb	2.9	0.9	0.5	1.5	0.8	1.3	1.4	0.6	0.9	4.0	124.6
Th	0.5	0.5	0.6	0.2	0.4	0.7	0.6	0.5	0.2	0.2	6.3
Pb	0.4	0.5	0.5	0.1	0.1	1.0	1.5	0.6	0.3	0.1	17.1
La	2	5	2	1	4	3	2	5	4	2	111†
Ce	10	12	9	6	5	8	8	8	10	4	249†
Nd	8	13	7	6	5	8	8	9	10	8	89†
Zn	105	108	101	89	88	124	89	107	78	111	70
Cu	115	175	160	156	152	146	182	137	194	170	9
Ni	63	91	59	83	81	73	76	74	93	102	12
Co	53	83	54	50	52	45	49	51	57	60	
Cr	91	120	92	179	180	148	123	130	147	206	6
V	377	438	374	333	328	389	368	397	362	376	63
Ba	16	12	11	9	10	13	14	9	8	0	2335
Sc	54	64	49	49	52	59	52	52	59	65	6
Ga	17	20	17	16	16	18	18	18	17	16	20

ted using depth as the vertical axis. The volcanic sequences plotted for Sites 917 and 918 represent, respectively, 770 m and 126 m of vertical section.

#### Site 917 Lower Series

The lowest lava flow at Site 917 sits on a thin layer of quartz sandstone overlying a steeply dipping metasedimentary unit. Interpretation of seismic sections (Fig. 3) suggests that approximately 300 m of the lower part of the volcanic succession has been removed by faulting (Larsen, Saunders, Clift, et al., 1994). Many of the flow units in

the lower part of the Lower Series are highly fractured, and intense brecciation was seen at the contacts of Units 71–72, 75–76, and 80–81 (Larsen, Saunders, Clift, et al., 1994). Thirty-five flow units were recognized in the Lower Series, of which 28 were analyzed in this study. One of these flows (Unit 71) gave a <sup>40</sup>Ar/<sup>39</sup>Ar plateau age of 60.4 ± 0.7 Ma (Sinton and Duncan, this volume). The flows range in composition from picrite (Unit 61B) to evolved tholeiite (Units 70, 71, 72, 74A, and 75A) with a general trend toward evolved compositions up the succession (Fig. 8). Peaks and troughs in Mg# and SiO<sub>2</sub> content suggest evolution of the magma in periodically recharged reservoirs (Larsen, Saunders, Clift, et al., 1994; Fitton et al., 1995).

**Table 5. NAA data (in ppm) for Leg 152 samples.**

Sample: Series:	915-3 Lava	917-10 Upper	917-14 Upper	917-17 Upper	917-32B Upper	917-33 Upper	917-34B Middle	917-47 Middle	917-55 Middle
La	2.3	1.8	0.9	5.7	1.5	3.3	18.6	46.8	49.9
Ce	6.1	6.0	3.0	14.2	5.1	10.4	41.2	91.4	99.6
Nd	5.4	6.6	3.6	10.8	4.6	9.7	23.4	39.0	43.0
Sm	2.05	2.53	1.71	3.38	1.52	3.18	5.91	6.25	7.59
Eu	0.86	1.06	0.78	1.33	0.65	1.26	2.09	1.79	1.86
Gd	3.1	3.6	2.9	4.5	2.0	4.1	6.7	4.7	6.1
Tb	0.66	0.68	0.56	0.83	0.36	0.73	1.13	0.64	1.01
Yb	2.83	2.16	1.97	2.55	1.10	2.19	3.54	1.61	2.91
Lu	0.46	0.32	0.31	0.38	0.17	0.33	0.51	0.24	0.42
Ta	0.12	0.08	0.02	0.13	0.07	0.14	0.33	0.24	0.47
Th	0.31	0.17	0.18	0.66	0.11	0.25	3.02	3.60	3.13
Hf	1.49	1.78	1.18	2.57	1.11	2.41	4.31	5.64	8.03
Sc	53.2	42.7	40.8	45.1	25.2	42.8	44.3	16.2	18.7
Co	52.4	60.1	81.4	50.7	92.1	53.0	42.8	22.7	18.7

Note: Concentrations not reported are below the detection limit.

**Table 5 (continued).**

Sample: Series:	917-60 Lower	917-61B Lower	917-62 Lower	917-68 Lower	917-70 Lower	917-72 Lower	917-74A Lower	917-78 Lower	917-81B Lower
La	6.4	5.0	4.8	9.1	17.8	40.1	38.3	8.5	9.3
Ce	16.7	11.6	11.5	20.5	38.4	80.0	84.0	18.3	21.5
Nd	12.2	8.3	8.1	13.4	20.2	38.0	43.0	11.0	13.2
Sm	3.73	2.29	2.22	3.34	4.48	7.67	8.55	2.55	3.42
Eu	1.44	0.93	0.93	1.33	1.62	2.60	2.79	0.98	1.31
Gd	4.6	2.7	2.7	4.1	5.3	7.4	8.4	3.3	4.0
Tb	0.81	0.47	0.45	0.67	0.80	1.16	1.36	0.50	0.72
Yb	2.36	1.31	1.28	1.98	2.33	3.22	3.83	1.73	2.22
Lu	0.39	0.20	0.20	0.31	0.35	0.45	0.62	0.25	0.32
Ta	0.44	0.30	0.29	0.52	0.81	3.15	0.41	0.12	0.16
Th	0.82	0.40	0.45	1.24	1.47	5.22	1.10	0.31	0.29
U						1.1			
Hf	3.86	1.53	1.55	2.94	3.81	6.98	7.13	1.46	2.33
Sc	42.3	28.2	27.0	38.2	33.4	25.5	28.1	32.6	34.9
Co	53.9	72.5	66.6	49.6	45.2	35.4	38.7	57.4	51.6

**Table 5 (continued).**

Sample: Series:	917-88 Lower	917-89 Lower	917-90 Lower	918-1 Sill	918-8B Lava	918-12Bi Lava	918-12Bii Lava	918-13B Lava	918-15 Lava
La	4.1	8.2	8.0	22.4	3.4	1.9	1.9	2.8	3.4
Ce	11.4	20.9	21.3	49.7	10.0	5.5	5.0	7.6	9.5
Nd	9.7	14.3	14.7	28.4	8.9	5.4	5.3	6.7	8.7
Sm	2.93	3.70	3.72	6.86	3.24	1.94	1.84	2.34	2.96
Eu	1.23	1.41	1.48	2.31	1.43	0.87	0.83	0.99	1.25
Gd		4.1		7.4	4.6	2.7	3.0	3.4	5.6
Tb	0.69	0.69	0.74	1.33	1.06	0.64	0.63	0.68	0.92
Yb	2.04	2.08	2.19	4.03	4.32	2.64	2.63	2.71	3.88
Lu	0.33	0.33	0.33	0.61	0.69	0.41	0.40	0.43	0.61
Ta	0.18	0.10	0.11	1.63	0.21	0.13	0.12	0.21	0.21
Th	0.27	0.24	0.22	2.12	0.28	0.19	0.20	0.31	0.32
U				0.5					
Hf	2.13	2.17	2.28	5.33	2.13	1.40	1.34	1.93	2.09
Sc	34.4	40.4	43.3	44.0	58.4	55.0	55.1	59.5	56.2
Co	78.8	52.8	56.1	50.9	71.5	58.2	61.2	52.3	57.3

At least two magma sources are represented in the Lower Series with respectively low and high Nb/Zr (Fig. 9). The six high-Nb/Zr flows are concentrated at the top of the Lower Series (Units 60, 61B, 62, 68, 70, and 72), intercalated with the more common low-Nb/Zr flows. Two units lower in the succession (78 and 92) also have slightly higher Nb/Zr. High-Nb/Zr units have generally higher concentrations of Rb, Th, Nb, and Ta than do the low-Nb/Zr units (Fig. 4), although the two groups are otherwise difficult to distinguish on the basis of their incompatible-element and REE patterns (Figs. 4, 6). The high- and low-Nb/Zr groups of flows both have basic and evolved members. The more silicic flows in both groups tend to have rather high Zr/Y and Ce/Y (Fig. 9), probably due to crustal assimilation. This will be discussed more fully in a later section.

Another striking feature of the Lower Series flows is their high and variable Ba/Zr, Sr/Zr, and La/Th (Fig. 10) compared with flows higher in the succession. Some of the scatter in Ba/Zr and Sr/Zr may be due to alteration, but the overall high values of the three ratios (es-

pecially La/Th) must be a primary magmatic feature and may also reflect crustal contamination.

#### *Site 917 Middle Series*

The top of the Lower Series is marked by a sudden change to more evolved compositions (Fig. 8). The Middle Series consists of 23 units of evolved tholeiite and dacite flows and welded and non-welded dacitic tuff. Four samples (two from Unit 34B, one each from Units 52 and 55) dated by Sinton and Duncan (this volume) gave  $^{40}\text{Ar}/^{39}\text{Ar}$  plateau ages within error of each other with a mean age of  $60.8 \pm 0.7$  Ma, the same as the date obtained from the Lower Series. Fourteen of the Middle Series units were analyzed in this study. The most evolved compositions are found at the base and toward the top of the series. Uniformly low Nb/Zr (Fig. 9) shows that the more enriched magmas represented in the Lower Series were absent. High Ce/Y and Zr/Y (Fig. 9), coinciding with peaks in  $\text{SiO}_2$  (Fig. 8), are most likely to be

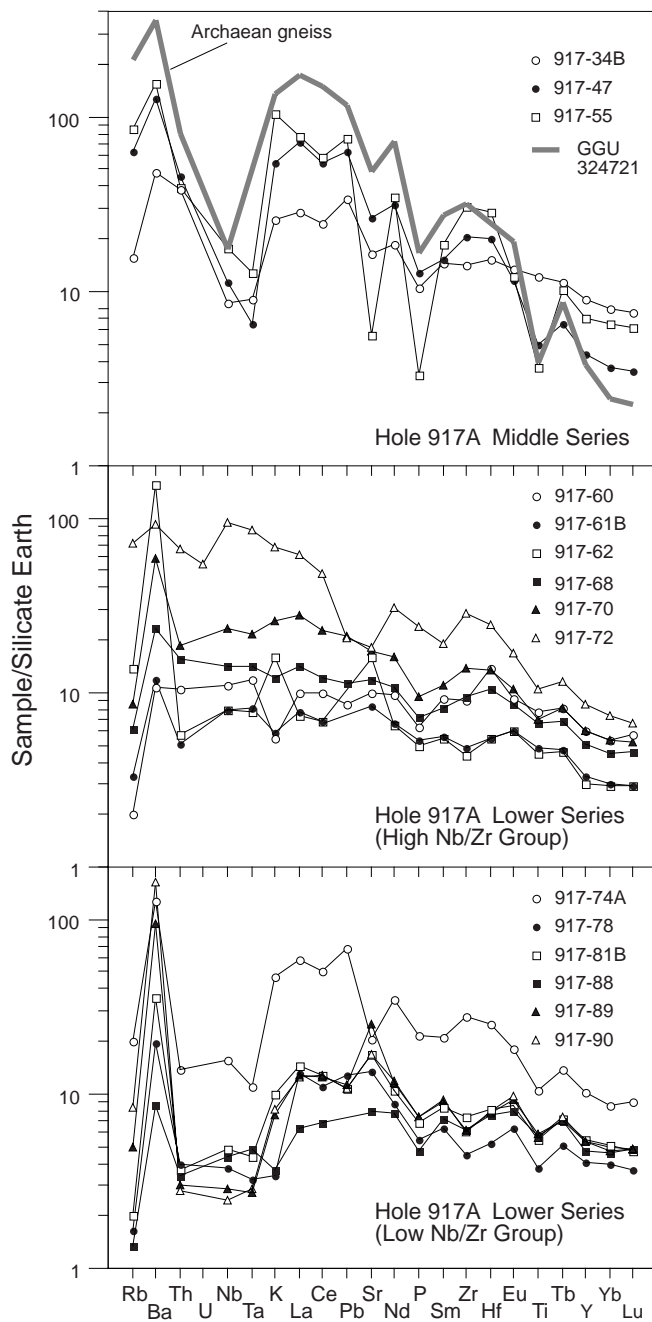


Figure 4. Normalized incompatible-element abundances in selected samples from Site 917, Lower and Middle Series. A sample of Archaean gneiss, collected from outcrop onshore close to the Leg 152 transect (GGU 324721, Blichert-Toft et al., 1995) is included for comparison. Abundances are normalized to primitive mantle values (McDonough and Sun, 1995).

due to crustal assimilation. High concentrations of Ti in some of the evolved tholeiite flows (e.g., Unit 34B; Table 4) imply that fractional crystallization also contributed to the evolution of the magma.

**Site 917 Upper Series**

A 67-cm sandstone unit marks a dramatic change from the thick silicic flows of the Middle Series to a sequence of 34 thin flow units (21 analyzed here) of olivine basalt and picrite forming the Upper Se-

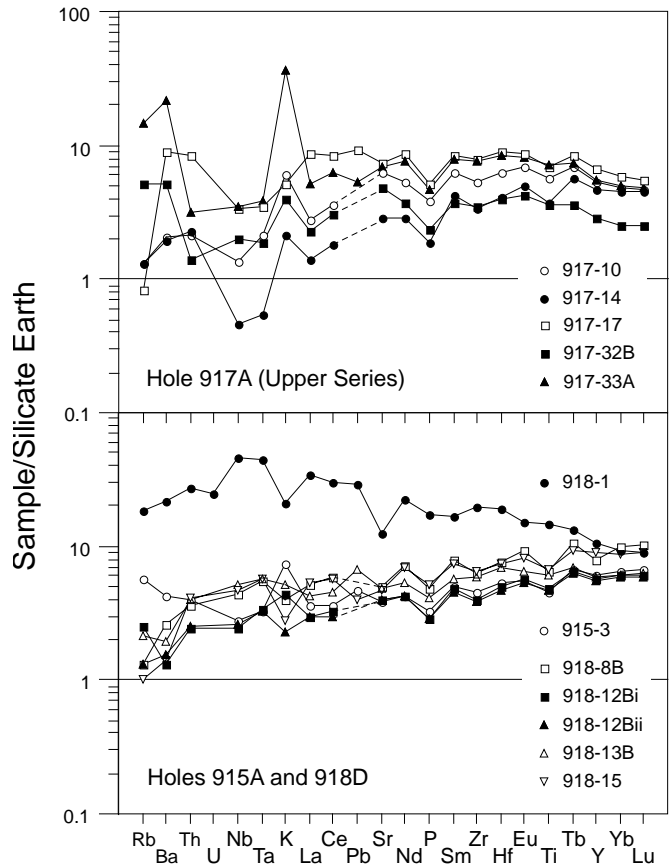


Figure 5. Normalized incompatible-element abundances in selected samples from Site 917, Upper Series, and Sites 915 and 918. Abundances are normalized to primitive mantle values (McDonough and Sun, 1995).

ries (Fig. 8). The time interval represented by this sandstone is unknown because it has not been possible to date any of the Upper Series samples.

Some of the more magnesian flows are strongly olivine-phyric and have clearly accumulated olivine. However, the high magnesium contents of the aphyric flows (18 wt% MgO, Mg# = 77 in 917-16), the high forsterite contents (up to Fo<sub>92</sub>; Demant, this volume) of the olivine phenocrysts, and the skeletal morphology of some of the phenocrysts, suggest that many of the units represent high-magnesium liquids close to primary magma in composition (Thy et al., this volume). The magma could not have been stored in large reservoirs for long periods, as inferred for the Lower and Middle Series, but was probably erupted rapidly through a system of fissures. This change in the style of magmatism may mark the final stage of breakup of the Greenland margin (Larsen, Saunders, Clift, et al., 1994; Fitton et al., 1995).

Compositional variation within the flows of the Upper Series is dominated by separation and accumulation of olivine, although there is some slight variation in incompatible-element ratios (Fig. 9). The flows become significantly more depleted (lower Zr/Y, Ce/Y, Nb/Zr) up the succession, and a group of five flows (Units 25, 26, 27, 31A, and 31B) near the base of the series have distinctly higher contents of incompatible elements in relation to their MgO contents than do the other flows (Larsen, Fitton, and Fram, this volume). Flows near the top of the succession (e.g., 917-10 and -14) are more depleted in light REE (LREE) than are flows from the base of the succession (917-32B and -33; Fig. 7). This variation may represent an increase, with time, in degree of melting or, alternatively, the effects of progressive depletion of the mantle reservoir feeding this volcanic system.

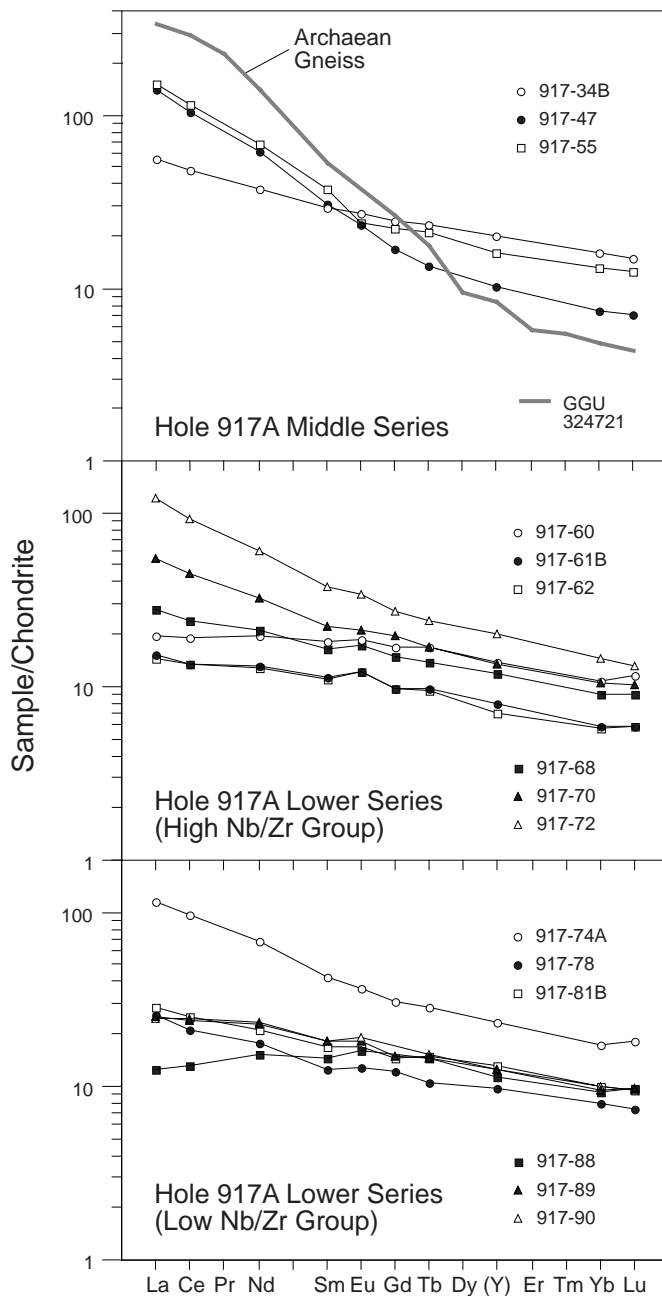


Figure 6. Chondrite-normalized REE abundances in selected samples from Site 917, Lower and Middle Series. A sample of Archaean gneiss, collected from outcrop onshore close to the Leg 152 transect (GGU 324721, Blichert-Toft et al., 1995) is included for comparison. Normalizing values are from Nakamura (1974).

#### Site 915 and 918 Lava Flows

The one lava flow recovered at Site 915 lies only 100 to 200 m higher in the succession than the top of Site 917 and yet it is compositionally quite different from the Upper Series lavas, but virtually identical to the lavas from Site 918, 70 km farther offshore. Consequently, the lava flows from these two sites will be considered together. Site 915 is on the continental shelf within the landward feather-edge of the SDRS, whereas Site 918 is on the continental rise, close to the center of the SDRS. Eighteen flow units were recovered from Site 918, 13 of which were analyzed. The top three flow units are

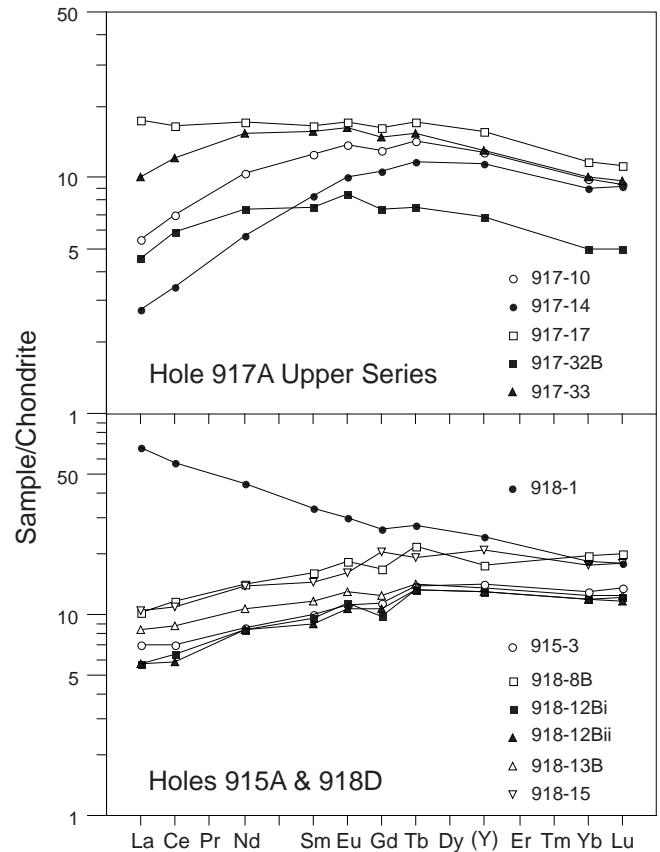


Figure 7. Chondrite-normalized REE abundances in selected samples from Site 917, Upper Series, and Sites 915 and 918. Normalizing values are from Nakamura (1974).

completely altered and reddened through deep subaerial weathering (Holmes, this volume), but the other flows are well preserved with only olivine and glass having been altered to clay. The basalt from Site 915 is fresh except for olivine, which has been completely altered. It has not been possible to date samples from either site.

Lava flows from Sites 915 and 918 have a very restricted composition (6.8–8.4 wt% MgO, 50.8–51.4 wt% SiO<sub>2</sub>, both calculated on a volatile-free basis, and omitting four samples with high LOI). Trace-element abundances and ratios are also very similar in lavas from the two sites, although the Site 915 basalt has slightly higher Ba/Zr (Figs. 5, 7, 9, 10), possibly due to slight crustal contamination. The narrow range of MgO content is similar to the range observed in mid-ocean-ridge basalt (MORB) from the North Atlantic Ocean (Schilling et al., 1983b). By the time the basalts sampled at Sites 915 and 918 were erupted, the rift system seems to have evolved toward the re-establishment of permanent magma reservoirs, this time in denser basaltic crust (Fitton et al., 1995).

#### Site 918 Sill

The highly weathered top of the lava pile at Site 918 is overlain by lower Eocene, shallow-marine glauconitic sands. These are apparently intruded by a thin sill composed of very fresh basalt (918-1). The contacts between basalt and sediment were not recovered and so the intrusive nature of this unit has not been firmly established. However, the unit is massive and vesicle-free and more likely to be intrusive than a lava flow. A sample from this unit gave a <sup>40</sup>Ar/<sup>39</sup>Ar plateau age of 51.9 ± 0.8 Ma (Sinton and Duncan, this volume), closely similar to the sediment age (53–51 Ma). The sill is clearly different in

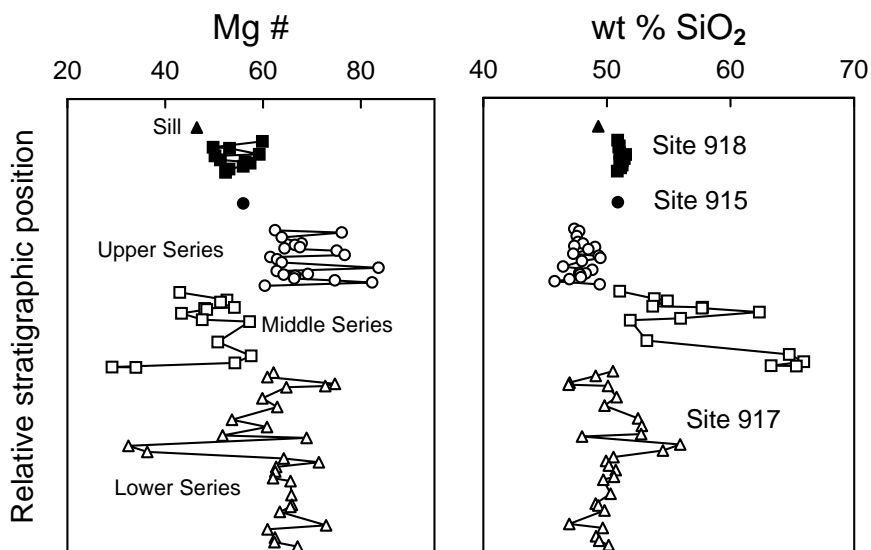


Figure 8. Stratigraphic variation of Mg# and SiO<sub>2</sub> in volcanic rock samples recovered from the Leg 152 transect. Data from the three sites are stacked to form a temporal and geographic sequence from the oldest and most landward at the bottom, to the youngest and most seaward at the top. The volcanic sequences plotted for Sites 917 and 918 represent 770 m and 126 m of vertical section, respectively. Mg# is 100MgO/(MgO+FeO) (molecular) where FeO is calculated from total Fe assuming Fe<sub>2</sub>O<sub>3</sub>/FeO = 0.15. SiO<sub>2</sub> was recalculated on a volatile-free basis with all Fe as FeO.

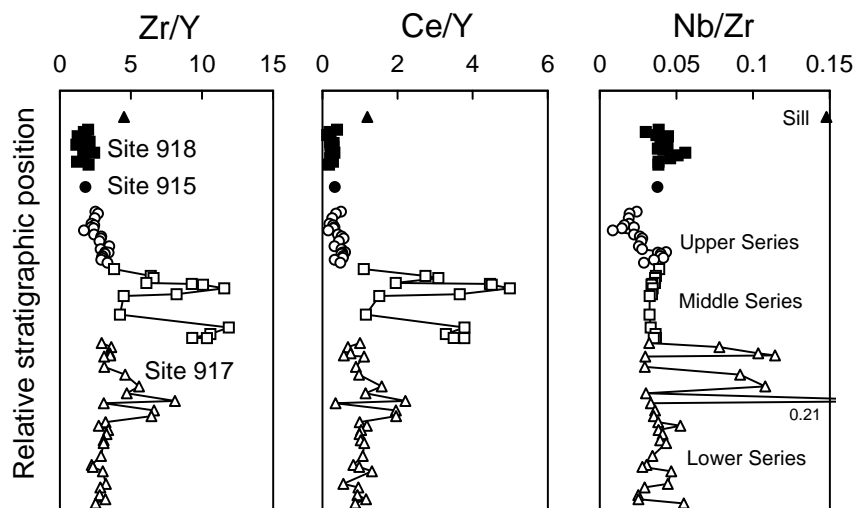


Figure 9. Stratigraphic variation of Zr/Y, Ce/Y, and Nb/Zr in volcanic rock samples from Leg 152. High Zr/Y, Ce/Y, and SiO<sub>2</sub> (Fig. 8) in the Middle Series reflects assimilation of Archaean crust. The bimodal distribution of Nb/Zr in the Lower Series implies the availability of magma from at least two mantle sources.

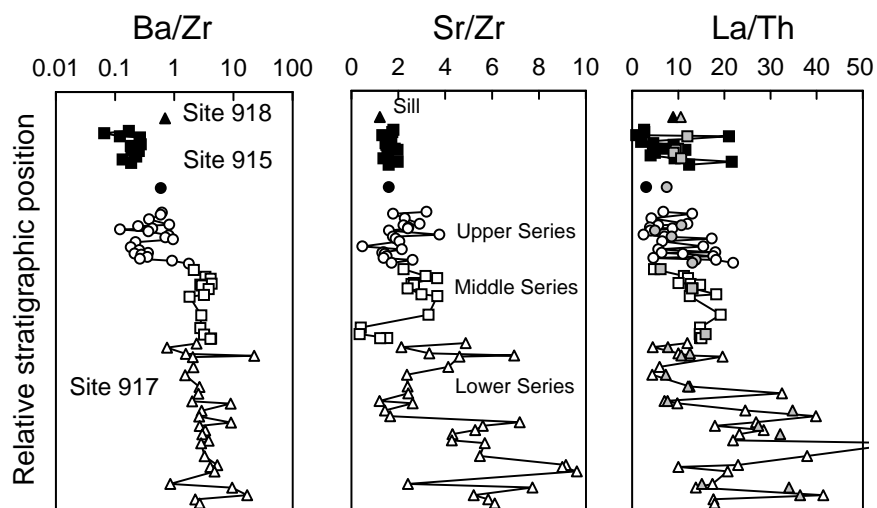


Figure 10. Stratigraphic variation of Ba/Zr, Sr/Zr, and La/Th in volcanic rock samples from Leg 152. The gray symbols on the La/Th plot represent NAA data and the other symbols XRF data. The decrease in these ratios through the Site 917 sequence may reflect the declining influence of lithospheric mantle or a lower crustal granulite contaminant.

composition from the underlying lavas (Figs. 5, 7–10) and is probably related to a small off-axis volcano seen in seismic profiles on top of the SDRS, just 3.5 km west of Site 918 (Larsen, Saunders, Clift, et al., 1994).

## PETROGENESIS

### Crustal Contamination

Correlated variation in  $\text{SiO}_2$  content,  $\text{Ce}/\text{Y}$ , and  $\text{Zr}/\text{Y}$  in samples from the Lower and Middle Series at Site 917 (Figs. 8, 9) cannot be explained by fractional crystallization of the observed phenocryst phases alone. Assimilation of a silica-rich crustal contaminant with high  $\text{Zr}/\text{Y}$  and  $\text{Ce}/\text{Y}$  is the most likely explanation for this variation. The contaminant must have low  $\text{Nb}/\text{Zr}$  since this ratio does not vary with  $\text{SiO}_2$  (Figs. 8, 9). A sample of Archaean gneiss, collected from an onshore outcrop close to the Leg 152 transect (GGU 324721, Blichert-Toft et al., 1995), has a composition similar to that inferred for the crustal contaminant, and an analysis of this sample is plotted along with those of representative Middle Series samples in Figures 4 and 6. The similarity in REE and other incompatible-element abundances between the gneiss sample and the more silica-rich Middle Series samples (917-47 and -55) is obvious. It is also clear that the more silica-rich members of the low- $\text{Nb}/\text{Zr}$  group from the Lower Series (e.g., 917-74A; Fig. 4) could also have been contaminated with Archaean gneiss. The Site 917 Upper Series and Site 915 samples appear to be relatively unaffected by contamination, and the Site 918 lavas were erupted, according to Larsen and Jakobsdóttir (1988), on oceanic crust. Much of the irregularity in the abundance patterns for these samples (Fig. 5) is in those elements susceptible to the effects of alteration, and the only clear evidence for contamination in the Upper Series lavas is the slight upturn at La and Ce in the REE pattern for 917-17 (Fig. 7).

Contamination with crustal material similar to sample 324721 cannot, however, explain the high  $\text{Ba}/\text{Zr}$ ,  $\text{Sr}/\text{Zr}$ , and  $\text{La}/\text{Th}$  seen in the lower units of the Lower Series (Fig. 10). Although the gneiss sample has ratios (7.0, 2.8, and 17.6, respectively) similar to those in the most silica-rich units of the Middle Series, the units comprising the bottom half of the Lower Series have much higher values (Fig. 10) and a contaminant with high  $\text{Ba}/\text{Zr}$ ,  $\text{Sr}/\text{Zr}$ , and  $\text{La}/\text{Th}$  would therefore be required. This is illustrated in Figure 11, which shows two distinct trends. One (toward sample 324721) extends to high  $\text{SiO}_2$  and  $\text{Ce}/\text{Y}$  at moderate  $\text{Ba}/\text{Zr}$ ,  $\text{Sr}/\text{Zr}$ , and  $\text{La}/\text{Th}$  (from Fig. 10), and the other to high  $\text{Ba}/\text{Zr}$ ,  $\text{Sr}/\text{Zr}$ , and  $\text{La}/\text{Th}$  at low  $\text{SiO}_2$  and low  $\text{Ce}/\text{Y}$ . The high-silica trend on Figure 11 can easily be explained by crustal assimilation coupled with low-pressure fractional crystallization. The latter will tend to increase  $\text{SiO}_2$  at constant  $\text{Ba}/\text{Zr}$  and  $\text{Ce}/\text{Y}$ , and reduce  $\text{Sr}/\text{Zr}$ .

The low-silica trend is less easy to explain. It is possible that the high values of  $\text{Ba}/\text{Zr}$  and  $\text{Sr}/\text{Zr}$  could be produced by alteration, but this is unlikely to be true for  $\text{La}/\text{Th}$ . Lithospheric mantle (e.g., Holm, 1988) and lower crustal granulite are both possible candidates for the contaminant. Some granulite-grade trondhjemitic gneisses from the Lewisian of northwest Scotland, for example, have high  $\text{Ba}/\text{Zr}$ ,  $\text{Sr}/\text{Zr}$ , and  $\text{La}/\text{Th}$  (Weaver and Tarney, 1980) coupled with high concentrations of Ba, Sr, and La. Depleted parental magmas could be strongly affected by amounts of contamination too small to increase the  $\text{SiO}_2$  content significantly. Alternatively, the low-silica trend could reflect interaction between asthenosphere-derived parental magmas, and Ba- and Sr-enriched lithospheric mantle. Whatever the cause of this trend, it is clear that its effects were confined to the lower part of the Lower Series (below Unit 73A). Above this level, contamination with gneisses similar to sample 324721 began to dominate the evolution of the magma, and the degree of this contamination increased through the Middle Series.

The Lower and Middle Series have recorded a temporal shift in the nature of the contaminant from lithospheric mantle, or lower crustal granulite, to upper crustal gneiss similar to sample 324721.

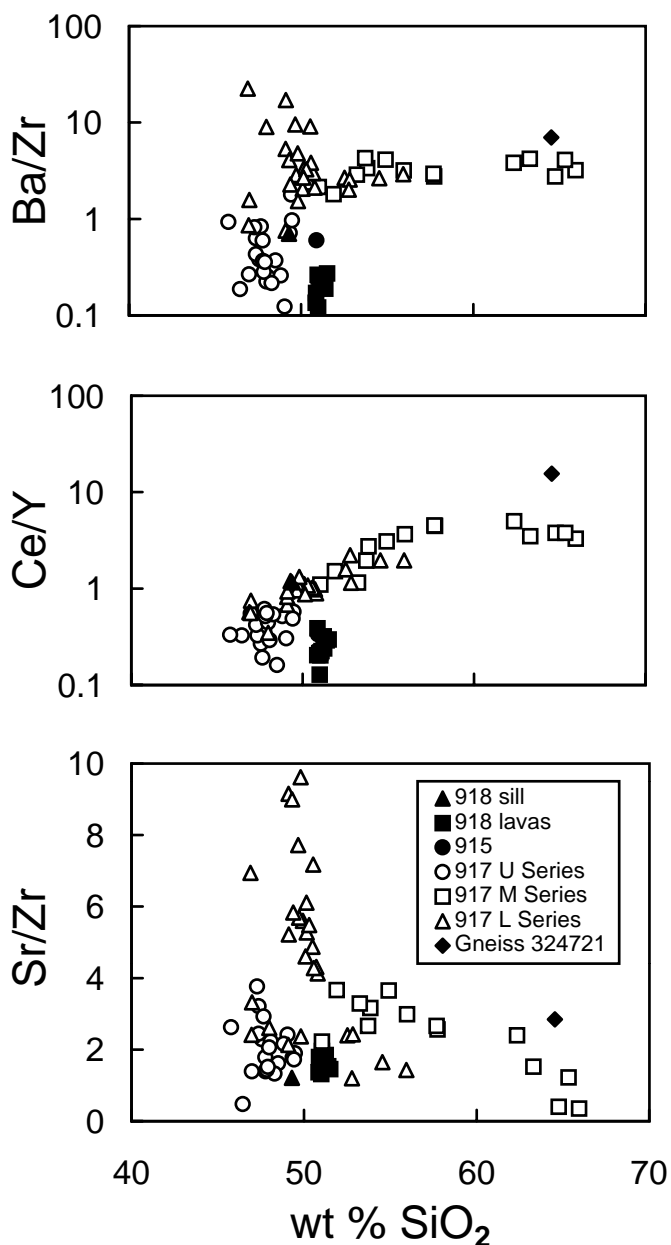


Figure 11. Variation of  $\text{Ba}/\text{Zr}$ ,  $\text{Sr}/\text{Zr}$ , and  $\text{Ce}/\text{Y}$  with  $\text{SiO}_2$  (recalculated on a volatile-free basis with all Fe as FeO). Two contamination trends are apparent. The trend extending to high  $\text{Ba}/\text{Zr}$  and  $\text{Sr}/\text{Zr}$  at constant  $\text{SiO}_2$  comprises the lower flows in the Lower Series (Fig. 10) and may reflect contamination with lithospheric mantle or lower crustal granulite. The trend extending toward the Archaean gneiss sample (324721) at high  $\text{SiO}_2$  comprises the upper flows in the Lower Series and the Middle Series silicic rocks. This trend represents contamination with upper crustal rocks.

This is analogous to the change in style of contamination demonstrated by Dickin et al. (1984) and Morrison et al. (1985) for the Scottish Tertiary igneous province. Dickin et al. (1984) showed that the proportion of lower crustal Pb in the inferred contaminant decreased, and the proportion of upper crustal Pb increased, with time during the development of the Skye intrusive complex. Isotopic studies on the Leg 152 samples (Fitton et al., this volume) show comparable and somewhat clearer temporal changes. The older Lower Series samples define a trend to low  $^{87}\text{Sr}/^{86}\text{Sr}$  and low  $^{143}\text{Nd}/^{144}\text{Nd}$ , while the younger Lower Series and Middle Series samples extend to high  $^{87}\text{Sr}/^{86}\text{Sr}$  and low  $^{143}\text{Nd}/^{144}\text{Nd}$ . This, together with an increase in  $^{208}\text{Pb}/^{204}\text{Pb}$  over

the same stratigraphic interval, suggests an increasing proportion of upper crust in the contaminant with time.

### Degree and Depth of Melting

It was noted earlier that the steady decrease in Zr/Y and Ce/Y in the Upper Series lavas may be due to an increase in degree of melting or progressive depletion of the mantle source with time. These alternatives can best be resolved through the use of moderately compatible elements sensitive to depth of melting, such as Sc. Figure 12 shows the variation of Sc and Zr in the Leg 152 volcanic rocks. Samples from the Middle Series at Site 917 and the more silica-rich samples from the Lower Series, all of which have probably been contaminated with continental crust, have been omitted. Sc is compatible in garnet lherzolite but slightly incompatible in spinel lherzolite; Zr is moderately incompatible in both. Equilibrium melting curves have been constructed using the following mineral-melt partition coefficients (D).

	$D_{Sc}$	$D_{Zr}$
Olivine	0.16	0.01
Orthopyroxene	0.33	0.03
Clinopyroxene	0.51	0.1234 (a)
Garnet	2.27	0.4 (b)

The values are from Ulmer (1989), except for (a), which is from Hart and Dunn (1993), and (b), which is a little higher than Ulmer's value (0.32) but at the lower end of the range (0.4–0.7) measured by Green et al. (1989). Ulmer's (1989) partition coefficients for pyroxenes and garnet were determined at 2.8 GPa and are therefore appropriate to mantle melting. Values of  $D^{spinel-liquid}$  have not been determined for Sc and Zr, and the effects of residual spinel have been ignored. Mantle phase proportions are taken from McKenzie and O'Nions (1991), and the proportions of phases entering the melt are from Johnson et al. (1990). Source concentrations of 7.5 ppm Zr and 12 ppm Sc, appropriate to moderately depleted mantle (McKenzie and O'Nions, 1995), were assumed. The resulting melting curves are sensitive to uncertainties in these parameters but serve to illustrate the variation in melting conditions with time.

The Site 917 Lower and Upper Series compositions cluster around the garnet lherzolite melting curve and imply about 3%–15% melting with only small amounts of subsequent crystallization. These values are close to those (4%–12%) deduced by Fram et al. (this volume) for the Upper Series magmas. Points to the left of the garnet lherzolite curve are consistent with accumulation of olivine phenocrysts. The arrows radiate from a point at 3 ppm Sc, 0 ppm Zr, and represent the effects of fractional crystallization of olivine (containing a small amount of Sc) and plagioclase. The five points around the upper arrow are from the group of flows close to the base of the Upper Series (Units 25, 26, 27, 31A, and 31B) with slightly higher incompatible-element concentrations in relation to their MgO contents.

The post-breakup lava flows (Sites 915 and 918) have higher Sc contents consistent with their derivation by 10%–20% melting of a shallower, spinel lherzolite source, followed by 20%–40% crystallization of olivine and plagioclase. If the source was more depleted in Zr than the 7.5 ppm assumed, the required degree of melting would be lower. However, the conclusion that the degree of melting became larger, and the depth of melt segregation shallower, as breakup proceeded is well constrained by the composition of the volcanic rocks (cf. Fram et al., this volume). A similar conclusion was reached by Fram and Leshner (1993) for the North Atlantic Tertiary igneous province as a whole, and by Thirlwall et al. (1994) for the Tertiary volcanic rocks of northeast Greenland. Both studies exploited the behavior of the heavy REE (HREE) to estimate the relative proportions of melt derived from garnet lherzolite and spinel lherzolite. HREE are relatively insensitive to the effects of crustal contamination and source

depletion, but are strongly fractionated by garnet. The effects of a decrease in depth of melting during continental breakup can be seen clearly in the REE patterns in Figures 6 and 7. All the Site 917 samples have a negative slope between Tb and Lu, implying the presence of residual garnet in the mantle source during the pre-breakup (Lower and Middle Series) and breakup (Upper Series) stages. By contrast, the post-breakup lava flows (Sites 915 and 918) have flat HREE patterns implying an absence of residual garnet.

The Sc contents of basaltic lavas from Sites 915 and 918 are unusually high and support the HREE evidence for shallow melting. The only other basaltic rocks in the North Atlantic region with such high Sc contents are the lavas from Hatton Bank (Fig. 12; data from Brodie and Fitton, this volume; Larsen, Fitton, and Fram, this volume). It is significant that Hatton Bank occupies a similar position to the Leg 152 transect on the conjugate North Atlantic margin (Fig. 1).

The sill from Site 918 has much higher concentrations of incompatible elements than any of the breakup and post-breakup lavas and must be the product of smaller degrees of melting. It was emplaced later than the lavas, probably from a nearby off-axis volcano. Its low MgO content and position on Figure 12 are consistent with its derivation by small degrees of melting of garnet lherzolite followed by crystallization of olivine, plagioclase, and augite. Scandium is compatible in calcic pyroxene at low pressure ( $D_{Sc} \approx 2.5$ , Gallahan and Nielsen, 1992), so fractional crystallization vectors for assemblages including augite would be much steeper than the ones shown.

### MANTLE SOURCES

One of the major objectives of Leg 152 was to investigate the nature of the mantle source for the SDRS at 63°N in order to determine whether the compositional and thermal effects of the Iceland plume were coupled or decoupled at the time of continental breakup (Larsen, Saunders, Clift, et al., 1994; Fitton et al., 1994). The present-day thermal anomaly, as expressed in water depth and major-element composition of dredged basalt, extends down the Reykjanes Ridge as far south as 50°N (Klein and Langmuir, 1987), but the chemical and isotopic anomaly can only be detected as far south as 60°N (Schilling, 1973; Schilling et al., 1983b; Hart et al., 1973). These effects reflect the steady-state condition of the Iceland plume today. The question to be addressed by Leg 152 was whether the plume was similarly zoned at the time of breakup. A more extensive compositional anomaly, with only a very thin carapace of heated ambient MORB mantle, would support the hypothesis that breakup was triggered by the impact, on the base of the lithosphere, of a start-up plume head originating at the core-mantle boundary (cf. Richards et al., 1989; Griffiths and Campbell, 1990). On the other hand, an extensive thermal anomaly with a smaller, concentric, chemical and isotopic anomaly, as at present, would be difficult to reconcile with this impact model. Such a thermal and compositional structure could support the hypothesis that the plume had been incubating beneath East Greenland for some time before breakup (cf. White and McKenzie, 1989; Kent et al., 1992). It would also be consistent with an origin of the plume at the 670 km discontinuity since such a plume could simultaneously tap mantle from below this level, to provide the compositionally anomalous center, and above it to provide the thermally anomalous carapace of MORB-source mantle.

Samples from Site 917 Upper Series and from Sites 915 and 918 are depleted in the more incompatible elements (Fig. 5) and in LREE compared with HREE (Fig. 7), implying that their mantle source was similarly, or more, depleted. Depletion in some incompatible elements (Rb, Th, Nb, Ta) is also apparent in the low-Nb/Zr group of the Site 917 Lower Series but not in the high-Nb/Zr group (Fig. 4). On simple compositional criteria, therefore, it looks as though two distinct mantle sources, one depleted and one less depleted, were involved in the formation of the SDRS at 63°N. However, these cannot be simply equated, respectively, with MORB mantle and Icelandic mantle. Strongly LREE-depleted basalt, with REE patterns similar to

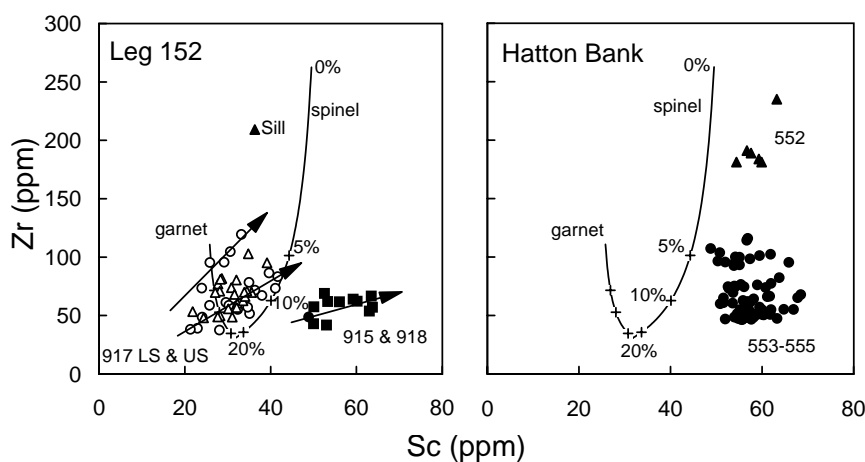


Figure 12. Variation of Sc and Zr in volcanic rocks from Leg 152 and Hatton Bank (Brodie and Fitton, this volume). Equilibrium melting curves, with percentage of melt, for garnet and spinel lherzolite are shown for reference. Arrows represent the effect of fractional crystallization of olivine and plagioclase. Variation among the Leg 152 samples reflects a temporal increase in degree of mantle melting, and decrease in depth of melt segregation. The Hatton Bank samples have extreme concentrations of Sc, comparable with the post-breakup lavas from Sites 915 and 918.

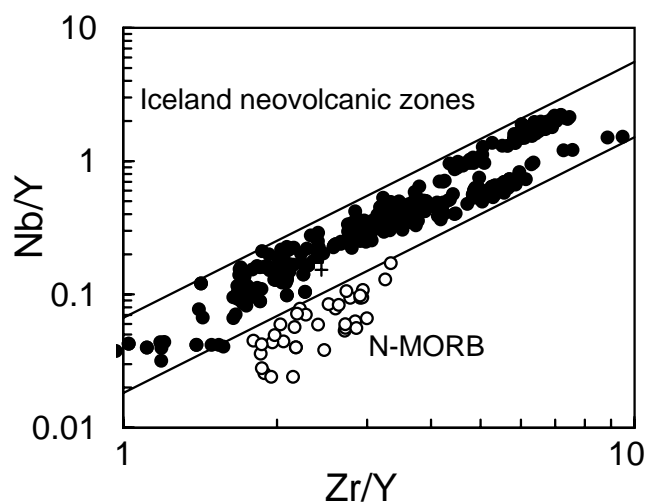


Figure 13. Nb/Y and Zr/Y variation in basalt from the neovolcanic zones of Iceland, compared with primitive mantle (+; McDonough and Sun, 1995), and typical N-MORB. The parallel lines mark the limits of the Iceland data. The Iceland samples cover the whole compositional range, from depleted picrite to alkali basalt, and were mostly analyzed by XRF in Edinburgh. Iceland data sources: western (including Reykjanes Peninsula), eastern, and northern rift zones: BSH and JGF (unpubl. data); Snaefellsnes Peninsula: Hardarson (1993); Vestmannaeyjar: Hardarson (1993) and Furman et al. (1991); Krafla: Nicholson (1990); Theistareykir: L. Slater and JGF (unpubl. data). N-MORB data sources: see Figure 15.

those from basalt erupted at normal segments of mid-ocean ridges (N-MORB), occurs in the neovolcanic zone of Iceland (Schilling et al., 1983a). Furthermore, contamination of magma of N-MORB composition with continental crust could produce LREE-enriched hybrid magmas with patterns resembling Icelandic basalt. A more subtle approach is required to distinguish magmas from N-MORB and Icelandic mantle sources.

The approach adopted here exploits the unusual behavior of Nb during the mantle melting processes responsible for the depletion of the N-MORB mantle reservoir. The abundance of most elements in the N-MORB source can be estimated through a simple mass-balance model in which average continental crust is subtracted from primitive mantle (e.g., McKenzie and O'Nions, 1991). This procedure fails to account for the low abundance of Nb in the N-MORB source, however, because both continental crust and N-MORB are depleted in Nb with respect to other incompatible elements; both have lower Nb/La than does primitive mantle, for example (Rudnick and Fountain, 1995; McDonough and Sun, 1995). Thus no mixture of continental

crust and N-MORB-source mantle can reproduce the Nb concentration in primitive mantle. The missing Nb is probably stored in subducted oceanic crust and ultimately recycled through some mantle plumes (Saunders et al., 1988). One effect of this process is that N-MORB is more depleted in Nb, with respect to other incompatible elements, than are even the most depleted Icelandic basalts. Furthermore, contamination of N-MORB magmas with continental crust can never produce hybrids resembling Icelandic basalts in their Nb contents.

Depletion of N-MORB in Nb, compared with Icelandic basalts and primitive mantle, is illustrated in Figure 13. The Iceland data cover the whole range of Icelandic basalt, from the most enriched off-axis alkaline basalts from Snaefellsjökull (Hardarson, 1993) to the most depleted picrites from the Reykjanes Peninsula, and include samples collected from the whole of the neovolcanic zone. Most of the Icelandic samples used in the construction of this diagram were analyzed by XRF in Edinburgh. The N-MORB data are from samples from 58°–59°N on the Reykjanes Ridge (R.N. Taylor, M.F. Thirlwall, and B.J. Murton, unpubl. data), the Pacific Ocean (ADS, unpubl. data), and average N-MORB compositions (Hofmann, 1988; Sun and McDonough, 1989). The Icelandic data form a remarkably linear array on this plot with upper and lower bounds defined by

$$\log(\text{Nb}/\text{Y}) = 1.92 \log(\text{Zr}/\text{Y}) - 1.176 \text{ (upper bound)} \quad (1)$$

and

$$\log(\text{Nb}/\text{Y}) = 1.92 \log(\text{Zr}/\text{Y}) - 1.740 \text{ (lower bound)}. \quad (2)$$

Primitive mantle (McDonough and Sun, 1995) plots within these bounds, and all the N-MORB data plot below the lower bound. The diagram is insensitive to fractional crystallization of olivine and plagioclase, typical of low-pressure evolution of primitive tholeiitic magmas, since crystal-liquid partition coefficients for Nb, Zr, and Y are close to zero in these phases (Pearce and Norry, 1979). Removal of augite, which has a significant partition coefficient for Y (Pearce and Norry, 1979), from more evolved tholeiitic magmas would drive the residual liquid away from the array at a shallower angle (at constant Nb/Zr). The data used in the construction of Figure 13, however, are all from basalt samples in which the effects of augite crystallization are insignificant. All the variation among Icelandic basalt due to differences in degree and depth of partial melting, including source depletion through melt extraction, are contained within the linear array. The diagram seems to provide a useful discriminant between basalt samples with N-MORB and depleted Icelandic mantle sources.

The Leg 152 data are plotted on the Nb/Y vs. Zr/Y diagram in Figure 14, along with data from the East Iceland Tertiary basalt pile

(BSH and JGF, unpubl. data). It is clear from this diagram that most of the samples from Site 917 plot below the lower bound of the Iceland field, in the region occupied by N-MORB (Fig. 13). The Site 917 Middle Series and some of the Lower Series samples fall on a linear trend toward the sample of Archaean gneiss (324721; Table 4). The identification of samples with an N-MORB mantle source is not complicated by assimilation of continental crust because this drives the magma away from the Iceland array. It is possible, on this plot, for a contaminated basalt with a depleted Icelandic mantle source to plot with N-MORB, but the resulting hybrid could be readily identified on other chemical criteria such as LREE enrichment. This is clearly not the case with the Site 917 Upper Series samples (Fig. 7). The six high-Nb/Zr samples from the Site 917 Lower Series, and the Site 918 sill, plot in the enriched part of the Iceland array (i.e., to the upper right of the primitive mantle composition), mostly within the field defined by Tertiary basalt from East Iceland. The two samples with slightly higher Nb/Zr (Fig. 9) from the lower part of the Lower Series plot just within the Iceland array. Basaltic lava samples from Sites 915 and 918 plot in the depleted part of the Iceland array.

Comparison plots for data from previous North Atlantic ODP and DSDP legs are given in Figure 15, with the N-MORB analyses used in Figure 13 for reference. Only the basalts from Hatton Bank, from the outer edge of the SDRS (Fig. 1), are truly N-MORB-like, as was noted by Joron et al. (1984) and Merriman et al. (1988). The Vøring Plateau basalts are transitional in character (cf. Viereck et al., 1988) and the more evolved lavas from the Vøring Plateau Lower Series show a similar crustal contamination trend to the Leg 152 data (Fig. 14). The basalt samples from Leg 49 plot entirely within the Iceland array. They were collected along a mantle flow line at 63°N, midway between Iceland and the outer limit of the compositional effects of the Iceland plume. They range in age from 2.3 Ma, close to the crest of the Reykjanes Ridge at Site 409, to about 35 Ma at Site 407 (Wood et al., 1979).

Data from other parts of the North Atlantic Tertiary igneous province are shown in Figure 16. The West Greenland picrites plot mostly below the Iceland array. This is an important observation because, like the Leg 152 and Hatton Bank lavas, the West Greenland picrites were erupted on the outer edge of the province (Fig. 1). Analyses of basalt samples from northeast Greenland, Scoresby Sund, and the lower formation of the Faeroes stray across the lower bound of the Iceland array, but not into the field occupied by N-MORB. Some of the upper basalts on the Faeroes are N-MORB-like in composition (Gariépy et al., 1983) but these account for only a small proportion of the lava pile. Data from the Faeroes lower basalt formation (Fig. 16) define a trend oblique to the Iceland array at constant Nb/Zr. A good positive correlation between Zr/Y and indices of differentiation in the Faeroes data led Bernstein (1994) to suggest that the magmas differentiated through crystallization of a garnet-bearing cumulus assemblage at lower crustal or upper mantle depths. Kerr and Thompson (1995), however, have challenged this conclusion and show that the observed variation in Zr/Y could be caused by fractional crystallization of olivine, plagioclase, and augite.

The data plotted in Figure 14 suggest that the source for the basalt samples collected during Leg 152 changed with time from N-MORB mantle (Site 917) to depleted Icelandic mantle (Sites 915 and 918). Basaltic magma with an undepleted Icelandic source was, however, available during eruption of the Lower Series and is represented most clearly by the six high-Nb/Zr samples (Fig. 9). A useful way to express the temporal variation in the mantle source is to calculate the excess or deficiency in Nb, using the lower bound of the Iceland array as a reference line. From Equation 1, the Nb/Y that a sample with a given Zr/Y would have if it were on the reference line is given by

$$\log(\text{Nb}/\text{Y})_{\text{RL}} = 1.92 \log(\text{Zr}/\text{Y}) - 1.740.$$

The deviation, in log units of Nb from this reference line ( $\Delta\text{Nb}$ ), is given by

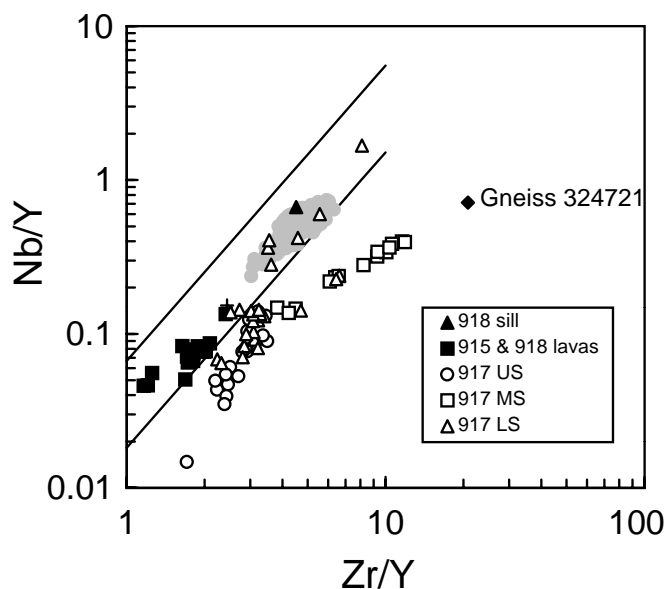


Figure 14. Nb/Y and Zr/Y variation in Leg 152 volcanic rock samples, compared with basalt from the East Iceland Tertiary lava successions (gray symbols; BSH and JGF, unpubl. data). Parallel lines defining the upper and lower bounds of the Iceland array (from Fig. 13), and the composition of primitive mantle (+), are shown for reference. The Middle Series and some Lower Series samples fall on a mixing line between uncontaminated basalt and the local Archaean gneiss (sample 324721; Table 4). This line is straight because the basalt and gneiss have the same Nb/Zr.

$$\Delta\text{Nb} = \log(\text{Nb}/\text{Y}) - \log(\text{Nb}/\text{Y})_{\text{RL}}. \quad (3)$$

A sample plotting on the reference line would have  $\Delta\text{Nb} = 0$ , one with 10 times the Nb content of a point on the reference line with the same Zr/Y would have  $\Delta\text{Nb} = +1$ , and one with one tenth the Nb content would have  $\Delta\text{Nb} = -1$ . The upper bound of the Iceland field (Eq. 1) has  $\Delta\text{Nb} = +0.564$ . Thus, positive values of  $\Delta\text{Nb}$  suggest an Icelandic mantle source and negative values an N-MORB mantle source.  $\Delta\text{Nb}$  is a mantle source characteristic and is insensitive to partial melting, source depletion through melt extraction, and to the effects of low pressure fractional crystallization of olivine and plagioclase. Figure 17 shows the variation of  $\Delta\text{Nb}$  with relative stratigraphic position, as in Figures 8–10, and shows clearly the transition from N-MORB mantle (negative  $\Delta\text{Nb}$ ) to Icelandic mantle (positive  $\Delta\text{Nb}$ ) sources between the top of the succession at Site 917 and the single flow recovered from Site 915. Periodic incursions of magma with an Icelandic mantle source during the eruption of the Lower Series at Site 917 are also seen in this plot. Some of the scatter in the data from Site 918 is due to the mobility of Y (Larsen, Fitton, Bailey, and Kystol, this volume), but this is not sufficient to detract from the conclusion that these lavas had a depleted Icelandic mantle source.

## CONCLUSIONS

Volcanic rock samples recovered during Leg 152 encompass the transition from continental flood basalt volcanism to the development of thick oceanic crust. Magma parental to the earliest volcanic rocks (Site 917, Lower Series) was stored in reservoirs where it evolved through a combination of fractional crystallization and assimilation of continental crust, culminating in the eruption of Middle Series dacite lavas and welded tuff. The oldest Lower Series lavas were contaminated with material with high Ba/Zr, Sr/Zr, and La/Th,

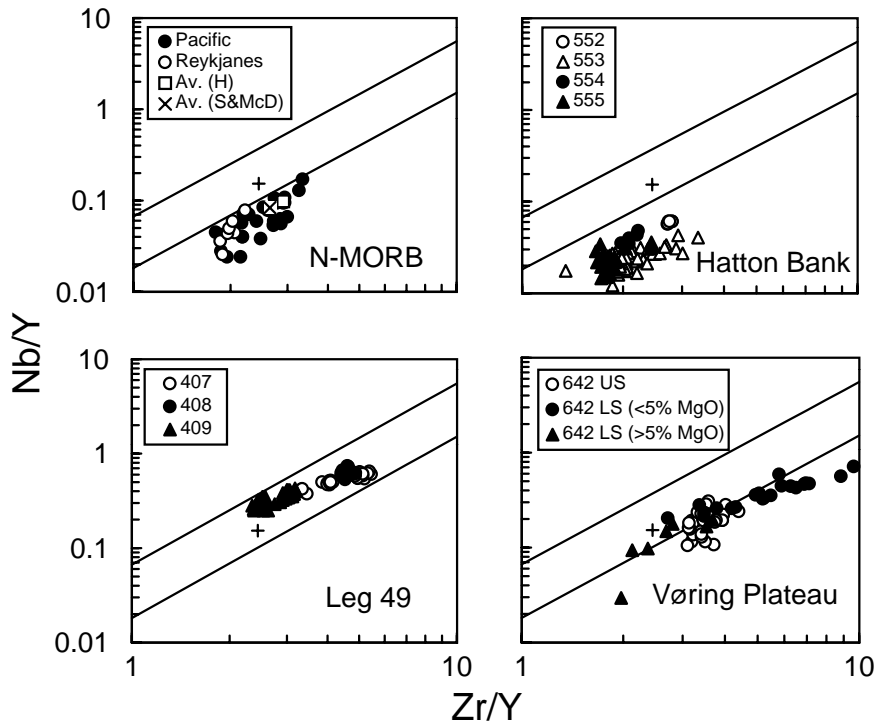


Figure 15. Nb/Y and Zr/Y variation in N-MORB and in volcanic rocks from previous North Atlantic DSDP and ODP legs. The parallel lines defining the upper and lower bounds of the Iceland array (from Fig. 13), and the composition of primitive mantle (+), are shown for reference. Data sources: Reykjanes Ridge N-MORB: R.N. Taylor, M.F. Thirlwall, and B.J. Murton (unpublished); Pacific N-MORB: ADS (unpublished, Nb calculated from Ta [ $\times 16$ ]); average N-MORB: Hofmann (1988) and Sun and McDonough (1989); Hatton Bank: Brodie and Fitton (this volume); Leg 49: Tarney et al. (1979); Vøring Plateau: Parson et al. (1989) and Viereck et al. (1989).

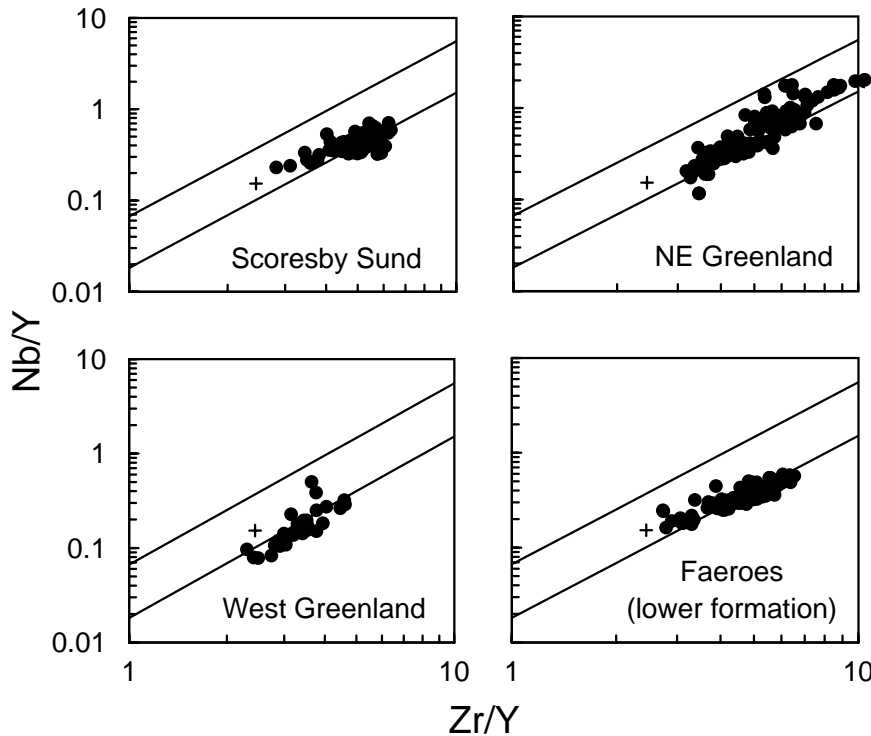


Figure 16. Nb/Y and Zr/Y variation in basaltic lavas from parts of the North Atlantic Tertiary igneous province. The parallel lines defining the upper and lower bounds of the Iceland array (from Fig. 13), and the composition of primitive mantle (+), are shown for reference. Data sources: Scoresby Sund: Larsen et al. (1989); NE Greenland: JGF and B.G.J. Upton (unpublished); representative analyses in Upton et al., 1984, and Thirlwall et al., 1994; West Greenland: Holm et al. (1993); Faeroes: Hald and Waagstein (1984).

consistent with lithospheric mantle or lower crustal granulite. The later volcanic rocks, however, appear to have been contaminated with upper crustal gneisses (Fitton et al., this volume). The magma reservoirs appear, therefore, to have moved to shallower levels in the crust with time. A similar shallowing of magma reservoirs has been suggested, on the basis of phase relations, by Fram and Leshner (1997) for the East Greenland Tertiary flood basalt province. The variation in the nature of the crustal contaminant with time is also very similar to that inferred for the Scottish Tertiary igneous province by Dickin et al. (1984) and Morrison et al. (1985).

The Middle Series evolved rocks are overlain by a thin sediment horizon that marks a pronounced shift in the character of magmatism. The overlying Upper Series is composed entirely of olivine basalt and picrite flows representing near-primary liquids with up to 18 wt% MgO (Thy et al., this volume). There is no evidence for long-term storage and differentiation of the magma, nor do the rocks show much evidence of interaction with the continental crust. It seems likely that the magma forming the Upper Series was erupted rapidly from mantle depths, through a series of fissures formed at the time of final breakup of the developing continental margin. A close coincidence in

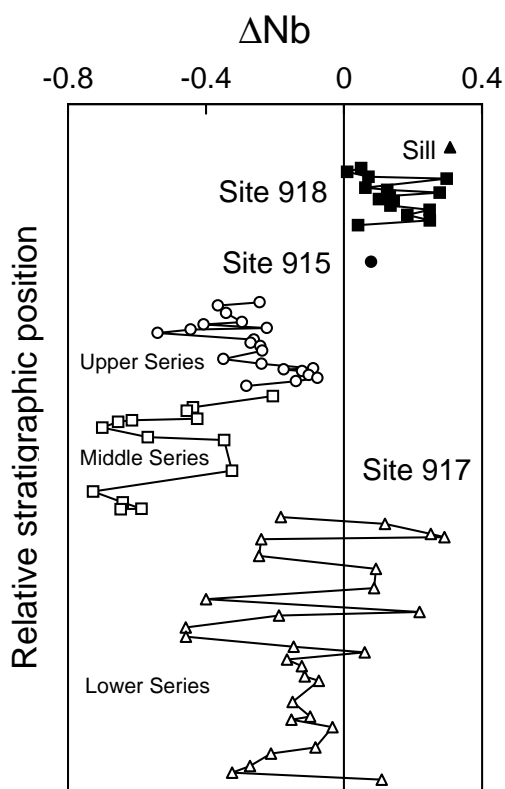


Figure 17. Stratigraphic variation of  $\Delta Nb$  in Leg 152 volcanic rock samples.  $\Delta Nb$  is the deviation, in log units, of Nb from the lower bound of the Iceland array (Fig. 13) and is a mantle source characteristic insensitive to partial melting, depletion through melt extraction, and to the effects of low pressure fractional crystallization of olivine and plagioclase. Positive values of  $\Delta Nb$  suggest an Icelandic mantle source, and negative values an N-MORB mantle source.

time between the eruption of picrite magma and the onset of seafloor spreading in East and West Greenland has been noted by Larsen et al. (1992).

No core was recovered from the stratigraphic interval between the top of the volcanic rocks at Site 917, and Site 915, 8 km farther offshore. The thickness of unsampled succession has been estimated from seismic data to be between 100 and 200 m (Larsen, Saunders, Clift, et al., 1994). Within this interval the character of volcanism changed again. The Site 915 basalt is virtually identical in its chemical composition to basalt recovered from Site 918, 70 km farther offshore and close to the center of the SDRS. A thin dike (Unit 39) intruding the Middle Series at Site 917 is very similar in composition to basalt from Sites 915 and 918 (Larsen, Fitton, and Fram, this volume). Basalt from Sites 915 and 918 has a very restricted composition (6.8–8.4 wt% MgO, 50.8–51.4 wt% SiO<sub>2</sub>, both calculated on a volatile-free basis) suggesting that, by the time these lava flows were erupted, the SDRS had evolved toward the re-establishment of permanent magma reservoirs, this time in denser basaltic crust in an oceanic spreading environment. As with mid-ocean ridges, the later SDRS magma reservoirs appear to have imposed a density filter to restrict the range of erupted magma compositions (Fitton et al., 1995).

The transition from continental to oceanic volcanism recorded during Leg 152 is the first to be described from a continental margin. However, Francis et al. (1983) described a virtually identical sequence from the Proterozoic Cape Smith fold belt of northern Québec. Here a sequence of continental flood basalts (the Povungnituk basalts) is related to continental rifting and shows evidence for storage, evolution, and contamination in crustal magma reservoirs.

These give way to a series of picritic basalts (the lower Chukotat Group) erupted rapidly through a conduit system dominated by fractures rather than magma reservoirs. The picrites are overlain by a sequence of basalts whose “compositional homogeneity ... implies the presence of large magma reservoirs, within or along the base of an oceanic crust, which buffered the compositions of the magmas rising from the underlying mantle.” The whole sequence is time-transgressive into the Cape Smith basin and remarkably reminiscent of the Leg 152 transect. Francis et al. (1983) speculate that their volcanic sequence was erupted on a developing continental margin.

As breakup proceeded from continental rifting to ocean crust formation, mantle melting extended to shallower depths. Lavas erupted during the rifting phase (Site 917) have low Sc contents, consistent with a garnet lherzolite source. After breakup (Sites 915 and 918) the Sc content increased markedly, implying that the magma segregated from a shallower, spinel lherzolite source. The Sc contents measured in the post-breakup basalts are unusually high and comparable with the highest values found in N-MORB (Klein and Langmuir, 1987). Within the North Atlantic igneous province, only the basalts from the SDRS at Sites 915 and 918 and on Hatton Bank have such high Sc contents (Brodie and Fitton, this volume; Larsen, Fitton, and Fram, this volume). The thickness of these SDRS implies large melt volumes, while the high Sc contents require that melting extended to unusually shallow levels. This combination of large degrees of melting at shallow depths may be a characteristic feature of SDRS erupted on the edge of the plume.

Langmuir et al. (1992) have evaluated the effects of the geometry of the melt region beneath spreading centers on the average degree and depth of melting and show that the largest-degree, shallowest melts should be produced by “active” upwelling. This occurs where partially molten mantle upwells faster than the rate of plate separation through, for example, melt-induced buoyancy, because all the mantle contributing partial melt is able to melt to the maximum degree at the shallowest level. Melting is more likely to occur by equilibrium than by fractional processes in this situation, hence the choice of equilibrium melting in the construction of Figure 12. Enhanced convection and consequent large-degree melting was proposed by Mutter et al. (1988) to explain thick volcanic sequences erupted soon after the initiation of seafloor spreading. These authors argue that enhanced convection is caused by the strong thermal contrast between the asthenosphere and the cooler steep edges of the pre-existing continental lithosphere. Active upwelling of the Iceland plume (e.g., Ribe et al., 1995), however, provides a much more likely mechanism for enhanced convection in the case of the Greenland continental margin. The data presented here support the notion of some form of enhanced convective mantle upwelling soon after continental breakup.

At least two mantle components were involved in the generation of the primary magmas responsible for the volcanic sequence sampled during Leg 152. Most of the earliest volcanic rocks (Site 917) had an N-MORB mantle source, although a few basalt flows toward the top of the Lower Series had an undepleted Icelandic mantle source. During the time interval represented by the short unsampled sequence (100–200 m) between the Upper Series olivine basalt and picrite flows, and the basalt lava flow at Site 915, the magma source changed from N-MORB mantle to depleted Icelandic mantle, and remained the same at Site 918. This transition coincided with the shallowing of mantle melting noted above. Basaltic lava flows sampled on Hatton Bank, closer to the outer edge of the SDRS, show the same evidence for shallow melting (Fig. 12) but had an N-MORB mantle source (Fig. 15).

These observations on the nature of the mantle source have implications for our understanding of the thermal and compositional structure of the Iceland plume at the time of its earliest magmatic expression. Basalt generated in the outer edge of the plume (sampled on Hatton Bank) had an N-MORB mantle source, and the Leg 152 basalts show a temporal transition from N-MORB to Icelandic mantle sources. Basalt erupted on the Vøring Plateau, closer to the inferred

plume axis, is transitional between N-MORB and Icelandic basalt. The Iceland plume was therefore zoned, much as it is today, with a core of compositionally and thermally anomalous mantle surrounded by a thick carapace of anomalously hot but compositionally normal N-MORB mantle. This observation is difficult to reconcile with the impact of a large plume head originating solely at the core/mantle boundary (Richards et al., 1989; Griffiths and Campbell, 1990). Such a plume would not have had time to heat its surroundings appreciably during its brief passage through the upper mantle and could have had, at most, only a very thin carapace of anomalously hot, N-MORB-source mantle. However, the apparently synchronous onset of magmatism at about 62 Ma across much of the North Atlantic igneous province (e.g., Saunders et al., in press) does suggest the initiation of the Iceland plume at this time, although Lawver and Müller (1994) have argued that the plume had been in existence before that time.

The arrival and rapid spread of a chemically and thermally zoned plume head originating at the 670-km discontinuity seems best able to explain the timing and compositional variation of magmatism in the North Atlantic igneous province. Decompression of the outer part of the plume head during continental breakup along the Leg 152 transect caused the N-MORB mantle in the outer part to melt first, followed by Icelandic mantle spreading out from the inner part. Previous melt extraction closer to the plume axis may account for depletion of the Icelandic mantle source of the post-breakup basalt lavas (Sites 915 and 918). Magma generated from Icelandic mantle was available from early in the sequence to supply the high-Nb/Zr lavas in the Lower Series at Site 917. This, together with the apparently abrupt transition from N-MORB-like basalt (Upper Series, Site 917) to depleted Icelandic basalt (Site 915), suggests that the interface between the two mantle sources was sharp rather than gradational.

## ACKNOWLEDGMENTS

Financial support for this research was provided by the Natural Environment Research Council (grant GST/02/673). We are grateful to Minik Rosing for supplying the gneiss sample 324721, and to Matthew Thirlwall for permission to use unpublished data from the Reykjanes Ridge. Andrew Kerr, Hans Christian Larsen, Bill Leeman, and Matthew Thirlwall are thanked for their thoughtful and constructive comments on the manuscript.

## REFERENCES

- Bernstein, S., 1994. High-pressure fractionation in rift-related basaltic magmatism: Faeroe plateau basalts. *Geology*, 22:815–818.
- Blichert-Toft, J., Rosing, M.T., Leshner, C.E., and Chauvel, C., 1995. Geochemical constraints on the origin of the late Archean Skjoldungen alkaline igneous province, SE Greenland. *J. Petrol.*, 36:515–561.
- Cande, S.C., and Kent, D.V., 1992. A new geomagnetic polarity time scale for the Late Cretaceous and Cenozoic. *J. Geophys. Res.*, 97:13917–13951.
- Dickin, A.P., Brown, J.L., Thompson, R.N., Halliday, A.N., and Morrison, M.A., 1984. Crustal contamination and the granite problem in the British Tertiary Volcanic Province. *Philos. Trans. R. Soc. London A*, 310:755–780.
- Eldholm, O., Thiede, J., Taylor, E., et al., 1987. *Proc. ODP, Init. Repts.*, 104: College Station, TX (Ocean Drilling Program).
- Fitton, J.G., Saunders, A.D., and Hardarson, B.S., 1994. Constraints on the nature of the Iceland plume from ODP Leg 152 (south-east Greenland volcanic rifted margin). *Mineral. Mag.*, 58A:272–273.
- Fitton, J.G., Saunders, A.D., Larsen, L.M., Fram, M.S., Demant, A., Sinton, C., and Leg 152 Shipboard Scientific Party, 1995. Magma sources and plumbing systems during break-up of the Southeast Greenland margin: preliminary results from ODP Leg 152. *J. Geol. Soc. London*, 152:985–990.
- Fram, M.S., and Leshner, C.E., 1993. Geochemical constraints on mantle melting during creation of the North Atlantic basin. *Nature*, 363:712–715.
- , 1997. Generation and polybaric differentiation of East Greenland Early Tertiary flood basalts. *J. Petrol.*, 38:231–275.
- Francis, D., Ludden, J., and Hynes, A., 1983. Magma evolution in a Proterozoic rifting environment. *J. Petrol.*, 24:556–582.
- Furman, T., Frey, F.A., and Park, K.H., 1991. Chemical constraints on the petrogenesis of mildly alkaline lavas from Vestmannaeyjar, Iceland; the Eldfell (1973) and Surtsey (1963–1967) eruptions. *Contrib. Mineral. Petrol.*, 109:19–37.
- Gallahan, W.E., and Nielsen, R.L., 1992. The partitioning of Sc, Y, and the rare earth elements between high-Ca pyroxene and natural mafic to intermediate lavas at 1 atmosphere. *Geochim. Cosmochim. Acta*, 56:2387–2404.
- Gariépy, C., Ludden, J., and Brooks, C., 1983. Isotopic and trace element constraints on the genesis of the Faeroe lava pile. *Earth Planet. Sci. Lett.*, 63:257–272.
- Govindaraju, K., 1994. 1994 compilation of working values and sample description for 383 geostandards. *Geostand. Newsl.*, 18 (spec. iss.).
- Green, T.H., Sie, S.H., Ryan, C.G., and Cousens, D.R., 1989. Proton microprobe-determined partitioning of Nb, Ta, Zr, Sr and Y between garnet, clinopyroxene and basaltic magmas at high pressure and temperature. *Chem. Geol.*, 74:201–216.
- Griffiths, R.W., and Campbell, I.H., 1990. Stirring and structure in mantle starting plumes. *Earth Planet. Sci. Lett.*, 99:66–78.
- Hald, N., and Waagstein, R., 1984. Lithology and chemistry of a 2-km sequence of Lower Tertiary tholeiitic lavas drilled on Suduroy, Faeroe Islands (Lopra-1). In Berthelsen, O., Noe-Nygaard, A., and Rasmussen, J. (Eds.), *The Deep Drilling Project 1980–81 in the Faeroe Islands*. Ann. Soc. Sci. Færoensis, 1984:15–38.
- Hardarson, B.S., 1993. Alkalic rocks in Iceland with special reference to the Snaefellsjökull volcanic system [Ph.D. dissert.]. Edinburgh Univ., UK.
- Hart, S.R., and Dunn, T., 1993. Experimental CPX/melt partitioning of 24 trace elements. *Contrib. Mineral. Petrol.*, 113:1–8.
- Hart, S.R., Schilling, J.-G., and Powell, J.L., 1973. Basalts from Iceland and along the Reykjanes Ridge: Sr isotope geochemistry. *Nature*, 246:104–107.
- Hofmann, A.W., 1988. Chemical differentiation of the Earth: the relationship between mantle, continental crust, and oceanic crust. *Earth Planet. Sci. Lett.*, 90:297–314.
- Holm, P.M., 1988. Nd, Sr and Pb isotope geochemistry of the Lower Lavas, East Greenland Tertiary Igneous Province. In Morton, A.C., and Parson, L.M. (Eds.), *Early Tertiary Volcanism and the Opening of the Northeast Atlantic*. Geol. Soc. Spec. Publ. London, 39:181–195.
- Holm, P.M., Gill, R.C.O., Pedersen, A.K., Larsen, J.G., Hald, N., Nielsen, T.F.D., and Thirlwall, M.F., 1993. The Tertiary picrites of West Greenland: contributions from “Icelandic” and other sources. *Earth Planet. Sci. Lett.*, 115:227–244.
- Jochum, K.P., Seufert, H.M., and Thirlwall, M.F., 1990. High-sensitivity Nb analysis by spark-source mass spectrometry (SSMS) and calibration of XRF Nb and Zr. *Chem. Geol.*, 81:1–16.
- Johnson, K.T.M., Dick, H.J.B., and Shimizu, N., 1990. Melting in the oceanic upper mantle: an ion microprobe study of diopsides in abyssal peridotites. *J. Geophys. Res.*, 95:2661–2678.
- Joron, J.L., Bougault, H., Maury, R.C., Bohn, M., and Desprairies, A., 1984. Strongly depleted tholeiites from the Rockall Plateau margin, North Atlantic: geochemistry and mineralogy. In Roberts, D.G., Schmitker, D., et al., *Init. Repts. DSDP*, 81: Washington (U.S. Govt. Printing Office), 783–794.
- Kent, R.W., Storey, M., and Saunders, A.D., 1992. Large igneous provinces: sites of plume impact or plume incubation? *Geology*, 20:891–894.
- Kerr, A.C., and Thompson, R.N., 1995. Comment on “High pressure fractionation in rift-related basaltic magmatism: Faeroe plateau basalts.” *Geology*, 23:671.
- Klein, E.M., and Langmuir, C.H., 1987. Global correlations of ocean ridge basalt chemistry with axial depth and crustal thickness. *J. Geophys. Res.*, 92:8089–8115.
- Langmuir, C.H., Klein, E., and Plank, T., 1992. Petrological systematics of mid-ocean ridge basalts: constraints on melt generation beneath ocean ridges. In Morgan, J., Blackman, D., Sinton, J. (Eds.), *Mantle Flow and Melt Generation at Mid-Ocean Ridges*. Geophys. Monogr., Am. Geophys. Union, 71:183–277.
- Larsen, H.C., and Jakobsdóttir, S., 1988. Distribution, crustal properties and significance of seaward-dipping sub-basement reflectors off East Greenland. In Morton, A.C., and Parson, L.M. (Eds.), *Early Tertiary Volcanism and the Opening of the Northeast Atlantic*. Geol. Soc. Spec. Publ. London, 39:95–114.
- Larsen, H.C., Saunders, A.D., Clift, P.D., et al., 1994. *Proc. ODP, Init. Repts.*, 152: College Station, TX (Ocean Drilling Program).

- Larsen, L.M., Pedersen, A.K., Pedersen, G.K., and Piasecki, S., 1992. Timing and duration of Early Tertiary volcanism in the North Atlantic: new evidence from West Greenland. *In* Storey, B.C., Alabaster, T., and Pankhurst, R.J. (Eds.), *Magmatism and the Causes of Continental Break-up*. Geol. Soc. Spec. Publ. London, 68:321–333.
- Larsen, L.M., Watt, W.S., and Watt, M., 1989. Geology and petrology of the Lower Tertiary plateau basalts of the Scoresby Sund region, East Greenland. *Bull.—Groenl. Geol. Unders.*, 157:1–164.
- Lawver, L.A., and Müller, R.D., 1994. Iceland hotspot track. *Geology*, 22:311–314.
- Leg 152 Shipboard Scientific Party, 1994. Drilling unearths “fire and ice” at southeast Greenland margin. *Eos*, 75:401–406.
- McDonough, W.F., and Sun, S.-S., 1995. The composition of the Earth. *Chem. Geol.*, 120:223–253.
- McKenzie, D., and O’Nions, R.K., 1991. Partial melt distributions from inversion of rare earth element concentrations. *J. Petrol.*, 32:1021–1091.
- , 1995. The source regions of ocean island basalts. *J. Petrol.*, 36:133–159.
- Merriman, R.J., Taylor, P.N., and Morton, A.C., 1988. Petrochemistry and isotope geochemistry of early Palaeogene basalts forming the dipping reflector sequence SW of Rockall Plateau, NE Atlantic. *In* Morton, A.C., and Parson, L.M. (Eds.), *Early Tertiary Volcanism and the Opening of the NE Atlantic*. Geol. Soc. Spec. Publ. London, 39:123–134.
- Morrison, M.A., Thompson, R.N., and Dickin, A.P., 1985. Geochemical evidence for complex magmatic plumbing during development of a continental volcanic center. *Geology*, 13:581–584.
- Mutter, J.C., Buck, W.R., and Zehnder, C.M., 1988. Convective partial melting, 1. A model for the formation of thick basaltic sequences during the initiation of spreading. *J. Geophys. Res.*, 93:1031–1048.
- Nakamura, N., 1974. Determination of REE, Ba, Fe, Mg, Na, and K in carbonaceous and ordinary chondrites. *Geochim. Cosmochim. Acta*, 38:757–776.
- Nicholson, H., 1990. The magmatic evolution of Krafla, NE Iceland [Ph.D. thesis]. Edinburgh Univ., UK.
- Norrish, K., and Hutton, J.T., 1969. An accurate X-ray spectrographic method for the analysis of a wide range of geological samples. *Geochim. Cosmochim. Acta*, 33:431–453.
- Parson, L., Viereck, L., Love, D., Gibson, I., Morton, A., and Hertogen, J., 1989. The petrology of the lower series volcanics, ODP Site 642. *In* Eldholm, O., Thiede, J., Taylor, E., et al., *Proc. ODP, Sci. Results*, 104: College Station, TX (Ocean Drilling Program), 419–428.
- Pearce, J.A., and Norry, M.J., 1979. Petrogenetic implications of Ti, Zr, Y and Nb variations in volcanic rocks. *Contrib. Mineral. Petrol.*, 69:33–47.
- Potts, P.J., 1986. *A Handbook of Silicate Rock Analysis*: Glasgow and London (Blackie).
- Reynolds, R.C., Jr., 1963. Matrix corrections in trace element analysis by X-ray fluorescence: estimation of the mass absorption coefficient by Compton scattering. *Am. Mineral.*, 48:1133–1143.
- Ribe, N.M., Christensen, U.R., and Theißing, J., 1995. The dynamics of plume-ridge interaction, 1: Ridge-centered plumes. *Earth Planet. Sci. Lett.*, 134:155–168.
- Richards, M.A., Duncan, R.A., and Courtillot, V.E., 1989. Flood basalts and hot-spot tracks: plume heads and tails. *Science*, 246:103–107.
- Roberts, D.G., Schnitker, D., et al., 1984. *Init. Repts. DSDP*, 81: Washington (U.S. Govt. Printing Office).
- Rudnick, R.L., and Fountain, D.M., 1995. Nature and composition of the continental crust: a lower crustal perspective. *Rev. Geophys.*, 33:267–309.
- Saunders, A.D., Fitton, J.G., Kerr, A.C., Norry, M.J., and Kent, R.W., in press. The North Atlantic igneous province. *In* Coffin, M.F., and Mahoney, J.J. (Eds.), *Large Igneous Provinces*. Am. Geophys. Union., Geophys. Monogr.
- Saunders, A.D., Norry, M.J., and Tarney, J., 1988. Origin of MORB and chemically depleted mantle reservoirs: trace elements constraints. *J. Petrol. (Spec. Lithospheric Iss.)*, 415–445.
- Schilling, J.-G., 1973. Iceland mantle plume: geochemical study of Reykjanes Ridge. *Nature*, 242:565–571.
- Schilling, J.-G., Meyer, P.S., and Kingsley, R.H., 1983a. Rare earth geochemistry of Iceland basalts: spatial and temporal variations. *In* Bott, M.H.P., Saxov, S., Talwani, M., and Thiede, J. (Eds.), *Structure and Development of the Greenland–Scotland Ridge: New Methods and Concepts*: New York (Plenum), 319–342.
- Schilling, J.-G., Zajac, M., Evans, R., Johnston, T., White, W., Devine, J.D., and Kingsley, R., 1983b. Petrologic and geochemical variations along the Mid-Atlantic ridge from 29°N to 73°N. *Am. J. Sci.*, 283:510–586.
- Sun, S.-S., and McDonough, W.F., 1989. Chemical and isotopic systematics of oceanic basalts: implications for mantle composition and processes. *In* Saunders, A.D., and Norry, M.J. (Eds.), *Magmatism in the Ocean Basins*. Geol. Soc. Spec. Publ. London, 42:313–345.
- Tarney, J., Saunders, A.D., Weaver, S.D., Donnellan, N.C.B., and Hendry, G.L., 1979. Minor element geochemistry of basalts from Leg 49, North Atlantic Ocean. *In* Luyendyk, B.P., Cann, J.R., et al., *Init. Repts. DSDP*, 49: Washington (U.S. Govt. Printing Office), 657–691.
- Thirlwall, M.F., Upton, B.G.J., and Jenkins, C., 1994. Interaction between continental lithosphere and the Iceland plume: Sr-Nd-Pb isotope geochemistry of Tertiary basalts, NE Greenland. *J. Petrol.*, 35:839–879.
- Ulmer, P., 1989. Partitioning of high-field strength elements among olivine, pyroxenes, garnet and calc-alkaline microbasalt; experimental results and an application. *Ann. Rep., Director Geophys. Lab., Carnegie Inst. Washington*, 1988–1989, 42–47.
- Upton, B.G.J., Emeleus, C.H., and Beckinsale, R.D., 1984. Petrology of the northern East Greenland Tertiary flood basalts: evidence from Hold With Hope and Wollaston Forland. *J. Petrol.*, 25:151–184.
- Viereck, L.G., Hertogen, J., Parson, L.M., Morton, A.C., Love, D., and Gibson, I.L., 1989. Chemical stratigraphy and petrology of the Vøring Plateau tholeiitic lavas and interlayered volcanoclastic sediments at ODP Hole 642E. *In* Eldholm, O., Thiede, J., Taylor, E., et al., *Proc. ODP, Sci. Results*, 104: College Station, TX (Ocean Drilling Program), 367–396.
- Viereck, L.G., Taylor, P.N., Parson, L.M., Morton, A.C., Hertogen, J., Gibson, I.L., and the ODP Leg 104 Scientific Party, 1988. Origin of the Palaeogene Vøring Plateau volcanic sequence. *In* Morton, A.C., and Parson, L.M. (Eds.), *Early Tertiary Volcanism and the Opening of the Northeast Atlantic*. Geol. Soc. Spec. Publ. London, 39:69–83.
- Weaver, B.L. and Tarney, J., 1980. Rare earth geochemistry of Lewisian granulite-facies gneisses, northwest Scotland: implications for the petrogenesis of the Archaean lower continental crust. *Earth Planet. Sci. Lett.*, 51:279–296.
- White, R., and McKenzie, D., 1989. Magmatism at rift zones: the generation of volcanic continental margins and flood basalts. *J. Geophys. Res.*, 94:7685–7729.
- White, R.S., Spence, G.D., Fowler, S.R., McKenzie, D.P., Westbrook, G.K., and Bowen, A.N., 1987. Magmatism at rifted continental margins. *Nature*, 330:439–444.
- Wood, D.A., Tarney, J., Varet, J., Saunders, A.D., Bougault, H., Joron, J.-L., Treuil, M., and Cann, J.R., 1979. Geochemistry of basalts drilled in the North Atlantic by IPOD Leg 49: implications for mantle heterogeneity. *Earth Planet. Sci. Lett.*, 42:77–97.

**Date of initial receipt: 5 September 1995**

**Date of acceptance: 3 August 1996**

**Ms 152SR-233**